2007-03-21

Lifetime Testing of Wire-Grid Polarizers with Selected Over-Coatings

Steven J. Malone
Brigham Young University - Provo

LIFETIME TESTING OF WIRE-GRID POLARIZERS WITH SELECTED OVER-COATINGS

by

Steven J. Malone

A thesis submitted to the faculty of

Brigham Young University

in partial fulfillment of the requirements for the degree of

Master of Science

School of Technology

Brigham Young University

April 2007

BRIGHAM YOUNG UNIVERSITY

GRADUATE COMMITTEE APPROVAL

of a thesis submitted by

Steven J. Malone

Each member of the following graduate committee has read this thesis and by majority vote has been found to be satisfactory.

Date	Barry M. Lunt, Chair
Date	C. Richard G. Helps, Member
Date	Ronald F. Gonzales, Member

BRIGHAM YOUNG UNIVERSITY

As chair of the candidate's graduate committee, I have read the thesis of Steven J. Malone in its final form and have found that (1) its format, citations, and bibliographical style are consistent and acceptable and fulfill university and department style requirements; (2) its illustrative materials including figures, tables, and charts are in place; and (3) the final manuscript is satisfactory to the graduate committee and is ready for submission to the university library.

Date

Barry M. Lunt
Chair, Graduate Committee

Accepted for the Department

Val D. Hawks
Director, School of Technology

Accepted for the College

Alan R. Parkinson, Dean
Ira A. Fulton College of Engineering
and Technology

ABSTRACT

LIFETIME TESTING OF WIRE-GRID POLARIZERS WITH SELECTED OVER-COATINGS

Steven J. Malone

School of Technology

Master of Science

Wire-grid polarizers (WGPs) offer superior extinction, durability, angle of incidence, and heat resistance when compared to traditional organic polarizers. WGPs are found in applications such as high lumen lighting, laser devices, high lumen digital cinema projectors, LED packaging, and other integrated optical applications and are driving the need for over-coatings. Over-coating a WGP has been found to increase lifetime and durability. This research provides lifetime data on coated and uncoated WGPs. WGPs over-coated with 100nm of SiO_2, 300nm of MgF_2, and with no over-coating were heated to temperatures of 450 ºC, 500 ºC, and 550 ºC and timed until they reached a predetermined optical failure point. The activation energies were calculated by applying the Arrhenius model to the failure data. WGPs with no over-coating were found to have an activation energy ≥ 1.5329 eV, with silicon dioxide an activation energy ≥ 1.7197 eV,

and with magnesium fluoride an activation energy ≥ 2.4577 eV. It has been shown that coating a WGP with an over-coating of silicon dioxide or magnesium fluoride slows the oxidation process of the aluminum nano-wires, thus increasing the lifetime of the WGP by 208% and 27,904%, respectively. Parasitic chemical reactions were not found to exist with silicon dioxide or magnesium fluoride when used as an over-coating.

ACKNOWLEDGMENTS

I wish to thank Dr. Barry Lunt, my committee chair, for his faith, mentorship, and encouragement throughout my graduate studies. I also wish to thank Ruth Ann Lowe for her help and support in seeing me through the program despite my many challenges. I also wish to thank MOXTEK for their financial support and use of their facilities and equipment. I am also thankful to Paul Mills, Dr. Ronald Gonzales, and Richard Helps for their editing and technical support. I am also thankful to Dr. Paul Kerry for his encouragement and support.

I would like to give special thanks to my wife, Jeanette, for her gentleness and wisdom in dealing with the needs of her husband, and for her many nights at home alone with our children (Hannah, Hyrum, Eli, Bethany, Isaac, and Ezra) while I studied.

TABLE OF CONTENTS

LIST OF FIGURES

1 Introduction

1.1 Background

Wire-grid polarizers (WGPs) offer superior extinction, durability, angle of incidence, and heat resistance when compared to traditional organic polarizers. WGPs are found in applications such as high lumen lighting, laser devices, high lumen digital cinema projectors, LED packaging, and other integrated optical applications and are driving the need for over-coatings. Wire-grid polarizers (WGPs) have long been used to polarize electromagnetic waves. As early as 1888 Heinrich Hertz used a wire-grid as a polarizer to test the properties of newly discovered radio waves (Hertz, 1893). Following Hertz, duBois and Rubens, in 1911, continued research on WGPs and extended their use into the far-infrared (Bird, 1960). The research of duBois and Rubens clearly established a connection between the physical spacing of the wires or pitch of the WGP and the smallest effective wavelength in which the WGPs could operate as a polarizer. In 1960 George Bird and Maxfield Parrish fabricated and tested a wire-grid polarizer for use in the near-infrared spectrum (Bird, 1960). The work of Bird and Parrish suggested that if the pitch of the WGP was small enough it could also be used as a polarizer in the visible spectrum. In 1998, MOXTEK Inc. of Orem, UT succeeded in developing a novel lithography technique that allowed for mass production of WGPs with a pitch small

enough to enable their use as a broadband polarizer in the visible, UV, and IR spectrums (Hansen, 1998).

Figure 1-1 is a magnified picture of a visible spectrum WGP.

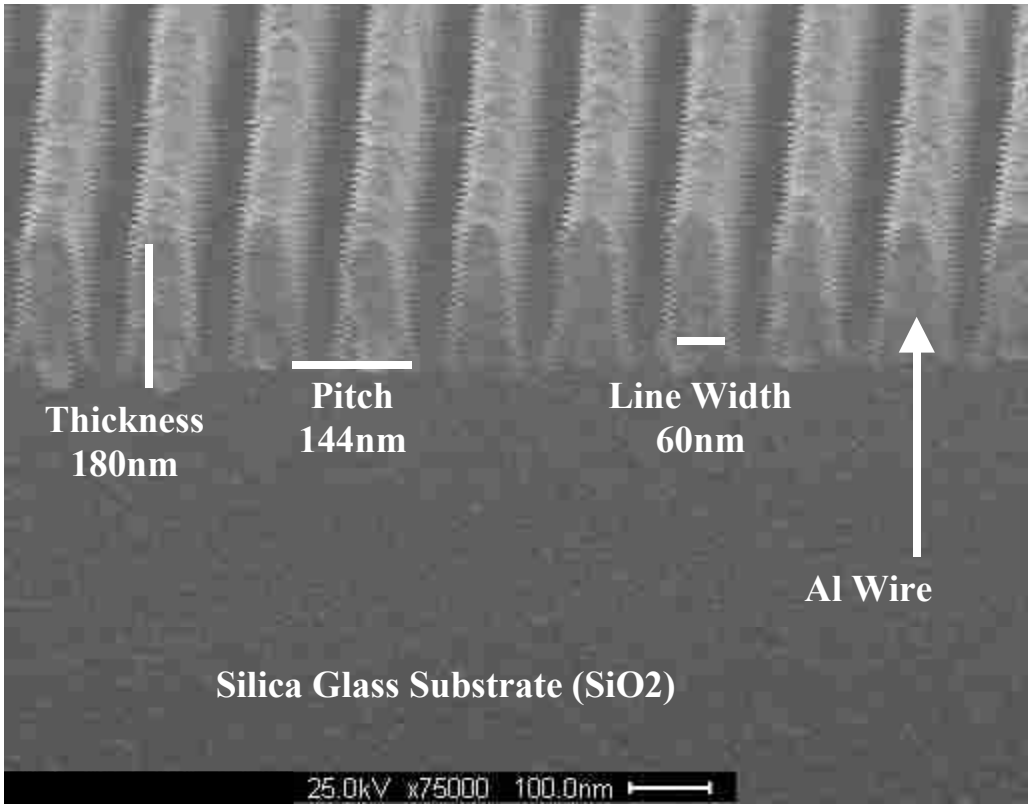

Figure 1-1 SEM picture of a WGP

Wire Height (Thickness): This term is defined as the thickness of the aluminum wires as determined by the desire to satisfy the following conditions: First, the aluminum thickness should be enough to be optically opaque and second, the aluminum thickness should be enough to achieve the desired transmission and extinction. The wire height of visible spectrum WGPs is typically between 100nm and 200nm

Line Width: This term is defined as the width of the aluminum lines that are on the surface of the glass. Typically the line width for visible spectrum WGPs is

approximately 60 nm although this may vary based upon the desired performance of the polarizer.

Duty Cycle: This term is defined as the line width divided by the pitch.

Pitch (Period): This term is defined as the distance between the leading edge of two consecutive lines. This is also called the period.

Visible spectrum wire grid polarizers (WGPs) are inorganic optical polarization devices made from parallel thin aluminum nano-wires placed on a glass substrate. Aluminum is generally the metal of choice for WGPs used in the visible spectrum (400nm to 700nm). This is because aluminum is highly reflective and absorbs only small amounts of electromagnetic energy in the visible region. The inorganic nature of the aluminum allows WGPs to withstand high temperatures that easily destroy organic thin film type polarizers. In addition to the benefit of heat resistance, the WGP is able to provide high polarization extinction along with high transmission efficiency. With organic thin film polarizers, transmission efficiency and contrast are usually traded one for the other depending on the application needs.

The glass substrate used is usually a Corning 1737F or equivalent type substrate material made primarily of SiO_2. The thickness of the substrate is usually between .2mm to 1.4mm. (ProFlux 2004)

Polarization extinction is defined as the ratio of desired to undesired polarization. WGP reflected extinction is defined as the intensity of the s-plane reflected waves divided by the intensity of the reflected waves not in the s-plane. WGP transmission extinction is defined as the intensity of the p-plane waves that are transmitted through the polarizer divided by the intensity of the waves not in the p-plane that are transmitted

through the polarizer. So, for example, if 1% of the total reflected light was not in the s-plane the extinction ratio would be 100:1, or it would have an extinction of 100 in the reflection mode. The transmission mode extinction would be calculated similarly. A common method of calculating WGP extinction is given by two the two equations: $Ts = I_s / I_p$ and $Tp = I_p / I_s$, where Ts is the reflected extinction, Tp is the transmitted extinction and I is the intensity of the s and p polarization states at a given wavelength.

Figure 1-2 is a magnified functional drawing of a WGP. When illuminated by non-polarized light, the nano-wires reflect s-polarized light and transmit p-polarized light.

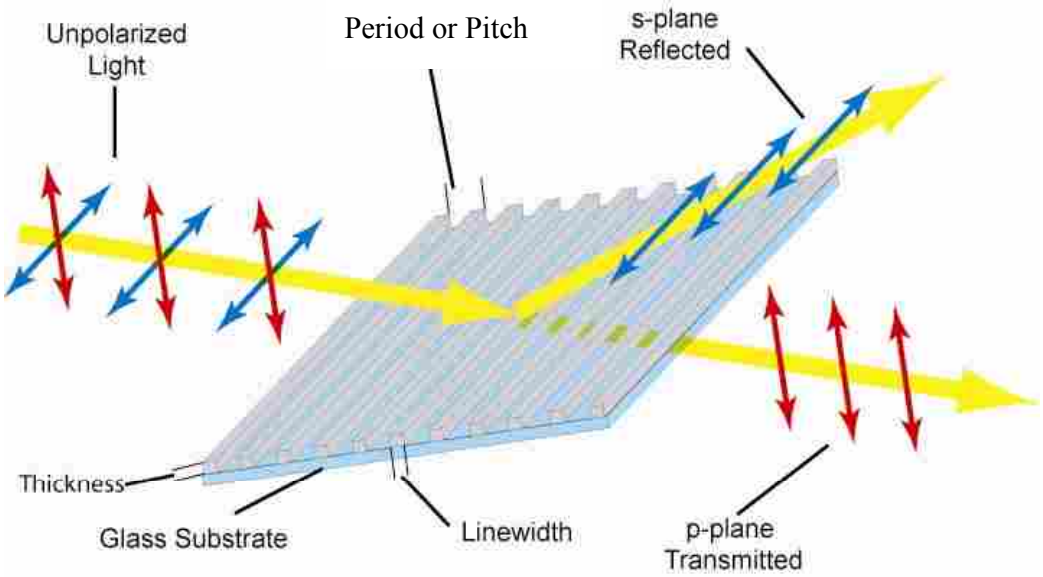

Figure 1-2 Magnified functional drawing of a WGP (picture courtesy of MOXTEK)

Electromagnetic waves with their electric field oriented orthogonal to the wires are transmitted through the polarizer while light with the electric field that is parallel to the wires is reflected or more precisely, radiated off of the wires. This phenomenon may seem counterintuitive. It is the result of the wires acting like antennas, absorbing and reradiating waves aligned with the wires. The wires work like a mirror for reflected s-

plane polarized light, and like a dielectric for the p-plane polarized light. Line width, thickness, and period independently and collectively affect the polarization extinction and optical efficiency of the WGP.

When measuring WGP extinction, the accuracy of the extinction measurement depends on several factors: the detector precision, analyzer alignment, stray light variations, and light source stability. Equation 1 is a formula for measuring visible spectrum WGP transmission extinction for a given wavelength, assuming a properly aligned sample and analyzer. (MOXTEK 2002)

$$T_{ex} = \frac{I_p - I_Z}{I_{oTp} - I_Z} \div \frac{I_s - I_Z}{I_{oTs} - I_Z} \qquad (1)$$

I_p represents the measured intensity of the light source measured through the sample with the analyzer oriented parallel to the sample's transmission axis (p-state analyzer). I_Z represents a background intensity reading with the main light source shuttered. I_{oTs} represents an intensity measurement of the light source through the s-state analyzer without the sample present. I_{oTp} represents an intensity measurement of the light source through the p-state analyzer without the sample present. I_o and I_Z measurements, taken for every extinction measurement, normalize and compensate for detector drift, light source drift, and stray light variations. In ideal extinction testing, without light source drift or detector drift or background noise variations, the I_{oTp} and the I_{oTs} would be equal to each other and would never drift together or apart and I_Z would be equal to zero. In this ideal case Equation 1 could be reduced to I_p / I_s.

WGP transmission efficiency is defined as the light throughput efficiency of the transmitted light through a WGP. In an ideal WGP 50% of the light intensity would be reflected in the s-polarization state and 50% transmitted in the p-polarization state and the polarizer would have a transmission efficiency of 100% and an infinite extinction. In application, WGPs have intrinsic transmission losses caused by substrate absorption and by the absorption of the aluminum nano-wires themselves. To calculate how much p-state light is transmitted through the sample Equation 2 is used:

$$Tp = \frac{I_p - I_Z}{I_{oTp} - I_Z} \qquad (2)$$

Tp is the calculated efficiency of the p-state light transmitted through the sample. I_p represents the measured intensity of the light source measured through the sample with the analyzer oriented parallel to the sample's transmission axis (p-state analyzer). I_Z represents a background intensity reading with the main light source shuttered. I_{oTp} represents an intensity measurement of the light source through the p-state analyzer without the sample present. Tp is usually expressed as a percentage, such as 89%. A transmission of 89% would indicate that 89% of the p-state light was transmitted through the sample.

For a WGP to work as an efficient polarizer in the visible spectrum, feature sizes such as pitch, duty cycle and aspect ratio, of the thin parallel aluminum wires, are important. Because of the complexity of manufacturing nano-sized features, there are currently only two methods capable of manufacturing visible spectrum WGPs, nano-imprint lithography and holographic lithography. Nano-imprint lithography WGP

manufacturing is based on using a master template, which has nano-features produced by e-beam lithography, to create a curable resist mold that enables nano-features to be dry etched into aluminum. (Wang 2005) The resist is cured by either heat or light. Nano-imprint manufacturing is currently more expensive than holography because of the expense of the template. Nano-imprint tools are versatile and are being used for research in optics, IC manufacturing, LED manufacturing, and most other research areas that require nano-scale features. Three companies are currently selling nano-imprint lithography tools that are capable of producing visible WGPs: Molecular Imprints, Nanonex, and Obducat.

The holographic lithography WGP manufacturing technique uses coherent light to create an interference pattern that is used to cure resist material to create the nano-structure. (Wang 2005) At the present, holography is a less expensive and less versatile manufacturing technique when compared to imprint lithography.

One feature size that is critical is the pitch, or periodicity of the wires. The pitch needs to be at least three times smaller than the smallest wavelength that is being polarized. If the pitch is greater than the wavelength divided by three, poor polarization extinction occurs. For example, to efficiently polarize a 400nm to 700nm wavelength spectrum a WGP would need to have a pitch of at least 133nm to work as an efficient polarizer for the entire spectrum. Many visible WGP applications work in the 450nm to 650nm spectrum and therefore, a pitch of at least 150nm is sufficient for those applications.

Another feature that is important in manufacturing WGPs is the duty cycle or fill factor. The duty cycle is the amount of space one wire occupies compared to the pitch.

If a wire has a width of 75nm and the pitch is 150nm the duty cycle would be 50%. The duty cycle range generally used to manufacture visible spectrum WGPs is from 40% to 60%. WGP duty cycle affects reflection and transmission efficiencies as well as reflection and transmission extinction ratios.

WGP aspect ratio is the wire thickness, measured from the glass substrate to the top of the wire, divided by the width of the wire. If the width of the wire is 60nm and the thickness of the wire is 180nm then the aspect ratio is 3:1. Most aspect ratios of visible spectrum WGPs are around 3:1. It is possible, however, to make visible WGPs with specific performance specifications from aspect ratios ranging between 2:1 and 25:1.

Visible spectrum WGP performance specifications vary according to pitch, duty cycle, and aspect ratio. It is important to consider the combination of efficiency and extinction when evaluating visible spectrum WGPs. When comparing the performance of one visible WGP to another, pitch, duty cycle, and aspect ratio along with efficiency and extinction should be considered.

Moxtek's WGPs have a pitch of 144nm with an aspect ratio of about 3:1 and a duty cycle of about 41%. The thickness of the wires approximately equals 180nm and the line width approximately equals 60nm. Moxtek produces three different products with slight structural variations in aspect ratio and duty cycle. Figure 2-5 shows current products offered by Moxtek with their corresponding performance specifications.

		450nm		550nm		650nm	
Product		Typical	Min/Max	Typical	Min/Max	Typical	Min/Max
PPL03C (General Purpose)	Tp (%)	85.7	84.0 Min	87.0	84.7 Min	86.1	84.2 Min
	Ts (%)	0.23	0.27 Max	0.14	0.16 Max	0.09	0.11 Max
	Contrast	370	310 Min	620	530 Min	950	760 Min
PPL04C (High Contrast)	Tp (%)	83.5	82.0 Min	84.9	82.0 Min	83.9	82.0 MIn
	Ts (%)	0.10	0.12 Max	0.08	0.10 Max	0.07	0.08 Max
	Contrast	835	680 Min	1060	820 Min	1200	1020 Min
PPLO5C (Very High Transmission)	Tp (%)	91.1	88.6 Min	92.5	90.0 Min	92.1	88.5 Min
	Ts (%)	0.52	0.89 Max	0.25	0.43 Max	0.15	0.26 Max
	Contrast	175	100 Min	370	210 Min	614	340 Min

Figure 1-3 MOXTEK WGP transmission performance specifications (courtesy of MOXTEK)

The pitch is the same for all of the products listed in Figure 1-3. The contrast shown is the same as extinction. Tp (transmission of the p-state light) is the desired transmission intensity percentage measured through the polarizer with respect to the intensity incident to the polarizer. Ts is the rejected (or unwanted polarization) intensity percentage measured through the polarizer with respect to the intensity incident to the polarizer. The contrast is figured by dividing Tp by Ts.

1.2 Problem Statement

WGPs are made of thin parallel nano-wires of aluminum placed on a transparent glass substrate. The delicate nano-wires are exposed to atmosphere on one side of the substrate, both during manufacturing and after installation in a final product. The exposed aluminum nano-wires are fragile and are easily damaged by standard assembly processes. The easily damaged nano-wires add increased complexity in the handling of the WGPs and in the assembly of products containing the WGPs. Therefore it is desirable and advantageous to have an over-coated WGP that is easier to handle and that is more robust.

In addition to the handling issues of exposed nano-wires, integrated optics is an emerging field with many products that require WGPs to be embedded. (Kostal 2003) WGP over-coatings are essential when making a planar surface for transitioning from a WGP nano-wire surface to another optical material surface. It is not currently known what effect over-coatings have on the lifetime of WGPs. It is assumed that over-coating will increase the lifetime of the WGPs, but there is reason to be concerned that possible parasitic chemical reactions between the over-coat and the nano-wires could reduce the lifetime of the WGPs.

1.3 Hypothesis

The null hypothesis is that over-coatings of 300nm of MgF_2 or of 100nm of SiO_2 will not affect the lifetime of the WGP they over-coat.

1.4 Justification

Polarization dependant technologies have much to gain by incorporating WGPs into their designs. WGPs offer superior extinction, durability, angle of incidence, and heat resistance when compared to traditional organic polarizers. Products utilizing WGPs that are currently being developed or are currently in production are: liquid crystal on silicon (LCOS) displays, high temperature poly-silicon (HTPS) displays, rear projection televisions (RPTVs), front projection televisions, DVD optical read/write heads, laser measuring devices, laser displays, optical encoders, 3D displays, 3D projectors, polarized light emitting diodes (LEDs), organic light emitting diodes (OLEDs), light pipes, micro-mechanical light modulators, anti-glare devices, ultra-violet (UV) alignment systems,

telescopes, optical beam splitting devices, polarimeter measurement devices, and various other sensors and measurement devices.

Understanding the effects of over-coatings on the lifetime of WGPs may help to optimize the WGP manufacturing process, further develop the WGP for increased lifetime, and supply necessary information needed to help optimize WGPs for integrated optical applications.

1.5 Methodology

As described earlier, an ideal WGP would have an infinite extinction, transmitting electric fields that are orthogonal to the wires and reflecting electric fields that are parallel to the wires. The ideal WGP would also have no insertion loss, transmitting and reflecting 100% of the incident light with no loss. When two ideal WGPs are physically positioned in a 90ºcrossed state, with the wires are perpendicular to each other, all of the incident light is blocked from being transmitted through the polarizers.

In practice, WGPs transmit some undesired polarization (Ts) and reflect some undesired polarization (Tp) and absorb some of the incident light.

The testing method consists of monitoring the samples undesired polarization transmission (Ts) as a function of accelerated heat aging. Tp is not measured or needed for this research. An intensity measurement is taken by using a WGP as an analyzer with its wires oriented 90º to that of the test samples wire orientation. As the test sample is aged by heat and begins to fail, the intensity measured through the WGP analyzer increases and the extinction of the test sample decreases. A failure point of Ts = .8% was chosen for each type of WGP sample tested; .8% represents less than 1% of the

undesired polarization state that was transmitted through the test sample. Three failure points for each type of sample have been obtained with associated temperatures and the time it took the sample to fail at that fixed temperature. Three time based failure points at temperatures of 450 ºC, 500 ºC, and 550 ºC have been obtained for each sample type at a wavelength of 550nm. Heat aged samples with MgF2, SiO2, and no over coating were compared.

1.6 Assumptions

It is assumed that the aluminum and glass materials used to make the polarizer samples were essentially the same in purity and physical structure from one sample to the next. This assumption is reasonable based on the consistency of the manufacturing process by which WGPs are made.

1.7 Delimitations

While WGPs polarize light in transmission and in reflection, this research was limited to the undesired transmitted polarization (Ts) measurements. The data analysis was limited to a single wavelength of 550nm. The measurements were limited to normal incidence measurements. The MgF_2 over-coating thickness will be limited to 300nm and the SiO_2 over-coating thickness will be limited to 100nm.

2 Review of Literature

2.1 Accelerated Testing

Accelerated testing shortens product life by subjecting the product to high stress. Stress is defined as any variable that causes degradation of a product, such as temperature, vibration, humidity, pressure, current, or voltage. Product degradation can be modeled as a force causing a deterioration reaction to occur. If a constant force is applied to a product and the product degradation can be measured over time, then the acceleration factor of the reaction can be calculated. With the known acceleration factor, the activation energy for the reaction can also be calculated. With the known activation energy, time based extrapolations based on the Arrhenius equation can be calculated. Accelerated lifetime testing (ALT) and highly accelerated lifetime testing (HALT) are both common methods of determining product failure modes and estimating product lifetimes.

2.1.1 ALT

Accelerated lifetime testing (ALT) is generally used to measure product reliability or degradation based on statistical methods. (Nelson, 2005) With ALT the product under test is observed under accelerated testing conditions and data is collected as degradation

happens over time. The more data that is available for statistical analysis the more accurate the predictions are. ALT is commonly used when a product has multiple failure modes and requires a detailed statistical examination to understand the data collected.

An example of ALT was published by Sontheimer, titled "Digital Micromirror Device (DMD) Hinge Memory Lifetime Reliability Modeling". This study used the Arrhenius acceleration model to predict the lifetime of a light modulation device. The DMD is a complex semiconductor-based micro-machine. The paper does not give details on the possible failure modes of the DMD. Some of the failure modes may be electro-migration, oxidation, or material fatigue. The ALT was conducted at temperatures ranging from 65 ºC to 95 ºC while the normal operation temperature was from 25 ºC to 45 ºC. The results of the ALT show a modest lifetime compared to actual field results. (Sontheimer, 2001) The author indicates that the model should be modified to reflect up-to-date actual field-testing. He gives these reasons why the model may be modest:

1. The DMD is operated normally at lower temperatures (some failure modes may not be present at the accelerated temperatures used in the ALT)
2. The DMD is typically not operated with a static image but with random images.
3. The average duty cycle experienced in the field is typically less stressful than the nearly full duty cycle of 5/95 used in the ALT.
4. The projectors are not operated continuously, thus allowing the stress in the hinge to relieve during off time.

ALT models are not perfect and are very specific to the product being tested. They produce lifetime predictions based on data collected by an experimental setup that may

not reflect actual conditions. ALT models should be modified and improved as time and data allow.

2.1.2 HALT

Highly accelerated lifetime testing (HALT) is used to force product failure for the purpose of product debugging or product development and is based on a more superficial statistical approach than ALT. (Nelson, 2005) HALT can also be used to determine product lifetime, but caution should be used when extrapolating data with possible multiple failure modes. "When multiple failure mechanisms are present, the overall activation energy corresponds to the minimum energy required to activate the weakest failure mechanism." (Groebel, 2001) The combination of multiple activation energies leads to modest lifetime estimates. Highly accelerated lifetime testing (HALT) typically uses temperature, vibration, humidity, or some combination of the three to find design weaknesses. Early discovery of weak links in prototype design is an important part of product development. HALT is a good method of determining product endurance limits, product failure modes, and, general lifetime estimates based on a single acceleration factor or a weighted average acceleration factor.

An example of HALT was published by Palcawich titled, "Highly Accelerated Lifetime Testing (HALT) of Lead Zirconate Titanate (PZT) Thin Films". This study used the Arrhenius acceleration model to calculate the activation energy of the PZT thin films. The HALT was set up to detect leakage current as a function of time at temperatures of 100 ºC, 120 ºC, 150 ºC, and 180 ºC. At 180 ºC the film failed after 0.036 hours. At 150 ºC it failed after 1.5 hours, at 120 ºC after 5 hours, and at 100 ºC after 20 hours. Extrapolated lifetime data was not provided, but failure mode analysis was. The

standard deviation of the natural logarithm of failure time was 0.6570. This standard deviation shows that the measured data fits the Arrhenius model. The activation energy was found to be 1.1eV.

Another example of HALT was published by Aubel, titled "Highly Accelerated Electromigration Lifetime Test (HALT) of Copper". In this study copper interconnects were held at constant temperatures of 300 ºC, 425 ºC, 450 ºC, and 475 ºC while unexpected resistance variations were measured at each temperature. A resistance increase of 20% was used as the criterion of failure. Two distinct failure types with distinct interconnect locations were discovered as a result of the HALT. Aubel notes that lifetime extrapolations to operating conditions should be done very carefully because of the two failure modes. Two distinct activation energies were discovered to be 0.81 eV for failure A and between 0.81 and 1.2 eV for failure B, with failure A having the lower activation energy of the two. Aubel also states that "To determine the temperature dependency of failure mechanism B, additional measurements at higher temperatures and an improvement in statistics will be necessary".

Like ALT models, HALT models are not perfect and are very specific to the product being tested. The HALT method only gives a summation of activation energies involved at a given temperature. It is not as critical for a HALT to represent the actual operating conditions to detect failure modes.

2.1.3 Challenges in HALT/ALT

Since the aim of HALT/ALT is to provide accurate life estimation and defect or design weakness, (Lall, 2004), it is important to search for unrecognized failure modes within a product. (Meeker, 1998) When a failure mode goes unnoticed, the resultant

lifetime prediction will be based on an activation energy that may never be a problem under normal circumstances. If the failure mode is noticed the activation energy can be accounted for and figured into the lifetime predictions. Another problem is that of unrealistic testing conditions. If a light bulb is tested under temperature conditions alone, the results will be erroneous. A light bulb is turned on and off; this switching greatly affects the life of the filament in the bulb. It is important to understand the nature of the failure. If a part is failing because of humidity and an HALT/ALT uses temperature alone as the stress component, it is possible for the product to have an extended life with increased temperature. Last of all, as we learned from the DMD example, drawing conclusions based on specialty-built prototype testing equipment may lead to incorrect conclusions.

2.2 Arrhenius Equation

The Arrhenius equation is a commonly used equation in calculating lifetime predictions based on accelerated heat testing. (Manca, 1999) Assuming the reaction speed is K, the Arrhenius equation can be expressed as: $K = A\ exp(-E_a/kT)$, where A is the proportional constant (that is characteristic of the chemical reaction), E_a is the activation energy, k is Boltzmann's constant (8.617385×10^{-5} eV/K), and T is temperature in Kelvin.

If a failure is assumed to happen when a certain degradation '$\boldsymbol{a}$' is reached, the lifetime can be expressed as $L = \boldsymbol{a}/K$. When $\boldsymbol{a}/A = A'$ is substituted, we have: $L = A'\ exp(E_a/kT)$. Because $\ln(L)$ and $1/T$ have linear interdependence, we can extrapolate lifetime data from two known temperatures and their related degradation. If we assume the lifetimes at temperatures T_1 and T_2 to be L_1 and L_2, the acceleration coefficient can be

obtained as: $L_2/L_1 = exp[(E_a/k)\cdot(1/T_2 - 1/T_1)]$. (Yang 2003) For example, let's assume that a light bulb has a lifetime of 10 hours when used in an ambient temperature of 400 Kelvin and, the same bulb has a lifetime of 1 hour when used in an ambient temperature of 475 Kelvin. What is the lifetime of the bulb when used in an ambient temperature of 300 Kelvin? If we let $E_a/k = E'$, the equation becomes $L_2/L_1 = exp[(E')\cdot(1/T_2 - 1/T_1)]$. Substituting lifetimes and associated temperatures gives: $E' = -5.833 \times 10^{-3}$ Kelvins. Now that we have E', we can solve for A' by using the lifetime equation $L = A' exp(E')$: $A' = 4.644 \times 10^{-6}$ hours. This gives us the equation $L = 4.644 \times 10^{-6}\ e^{(5833\ k/T)}$ for a temperature T in Kelvins. The predicted lifetime at 300 Kelvin would be 1209.3 hours. This is assuming that the mechanism of failure is the same at 300 Kelvin, 400 Kelvin and, at 475 Kelvin.

2.2.1 Activation Energy

Each failure mechanism has a unique activation energy. The activation energy is the energy, measured in electron volts, that is required to activate a process which degrades a product.

2.3 Aluminum WGP Heat Testing

Literature reporting heat testing or accelerated testing of WGPs is rare. One reference stated, "Heat testing has been conducted on WGPs for 1000 hours at 200 ºC with less than one percent change in transmission and less than four percent change in extinction." (Kahn) No other mention of heat testing or accelerated testing of WGPs has been found to be published or is known to exist.

2.4 WGP Failures

WGPs are dependant on the electrical characteristics of the aluminum nano-wires to function effectively as a polarizer. As aluminum oxidizes it changes from a conductive material to a dielectric material. There are two types of WGP failures: degradation failures, and catastrophic failures. Catastrophic failures are caused by improper handling of the WGP and result in physical destruction on the nano-wires or the substrate. Degradation failures are caused by aluminum oxidation. The rate at which aluminum oxidizes is directly proportional to the temperature of the WGP; the higher the temperature the faster the oxidation occurs.

2.5 Summary

Because WGP degradation failures do not occur under normal stress conditions within a reasonable amount of time, accelerated testing is needed to produce premature failures. Accelerated testing is useful in determining design weaknesses and lifetime estimates. Caution should be taken when HALTs are conducted for the purpose of predicting long term product reliability. HALT testing can produce degradation that would not normally be present in normal use conditions. HALT is a fast method of failure mode analysis and can give rough estimates of lifetime when failure modes are known under normal testing conditions. ALT strength is in statistical analysis of degradation points along a failure path. The failure path does not necessarily need to achieve actual failure, but the more data over long lengths of time produce better lifetime models. ALT also is used with complicated degradation models that have multiple activation energies and multiple failure modes to interpret the data.

3 Research Procedures

3.1 Visible Spectrum WGP Measurement Theory

When randomly polarized light is transmitted through a WGP, the resulting electric vector can be modeled as having two components, an electric vector associated with the p-state waves and an electric vector associated with the s-state waves that are each scaled by a scalar value. The scalar value is proportional to the square root of the intensity associated with each polarization. Equation 3 is the resulting electric vector equation for unpolarized light passing through a WGP. It includes the transmitted p-state and s-state electric vectors with their scale values.

$$\vec{E}' = t\left(\hat{p}\cdot\vec{E}\right)\hat{p} + c\left(\hat{r}\cdot\vec{E}\right)\hat{r} \qquad (3)$$

In Equation 3, $\vec{E}'$ is the resulting electric vector that is transmitted through a WGP. The scalar value for the p-vector electric field is t and the scalar value for the s-vector electric field is c. Because the light is unpolarized, the electric field in the p-direction $\left(\hat{p}\cdot\vec{E}\right)\hat{p}$ is equal to the electric field in the orthogonal direction $\left(\hat{r}\cdot\vec{E}\right)\hat{r}$. Thus, the dot products in Equation 3 both yield $\frac{E}{\sqrt{2}}$ to give $\vec{E}' = t\left(\frac{E}{\sqrt{2}}\right)\hat{p} + c\left(\frac{E}{\sqrt{2}}\right)\hat{r}$.

In Figure 3-1, with intensity I_0 normally incident upon polarizer P (sample to be measured) I_1 is the resulting intensity after passing through polarizer P. I_1 is normally incident upon analyzer A, and I_2 is the resulting intensity of I_1 after passing through the analyzing polarizer A.

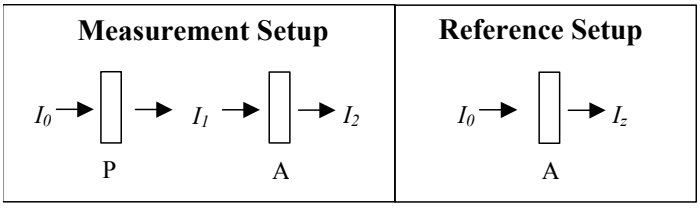

Figure 3-1 Measurement and reference setup for determining polarization performance of polarizer P with analyzer A. (courtesy of Moxtek)

Reference measurement I_z, in Figure 3-1, is needed to obtain the transmission efficiency of the p-state polarization. The reference measurement electric field vector is equal to $\vec{E}_z = t\left(\frac{E_o}{\sqrt{2}}\right)\hat{p} + c\left(\frac{E_o}{\sqrt{2}}\right)\hat{r}$. If we factor out $\frac{E}{\sqrt{2}}$ we are left with $\vec{E}_z = \frac{E_o}{\sqrt{2}}\left(t_A\hat{p}_A + c_A\hat{r}_A\right)$. Converting the electric field vector to intensity is accomplished by squaring the magnitude of the electric field vector yielding $I_z = \frac{E_o^2}{2}\left(T_A + C_A\right)$. Then, factoring out T_A we are left with $I_z = \frac{E_o^2}{2}T_A\left(1 + \frac{1}{R_A}\right)$ or, factoring out C_A leaves us with $I_z = \frac{E_o^2}{2}C_A\left(R_A + 1\right)$. When using a polarizing analyzer A to find the extinction of a sample polarizer P, as shown in Figure 3-2, a cross-polarization intensity measurement is necessary. In Figure 3-2, we see that I_{2p} (Tp) is the resulting intensity when P and A are aligned with their transmission axis parallel to each other and I_{2r} (Ts) is the resulting intensity when the transmission axis of A is orthogonal to the transmission axis of P.

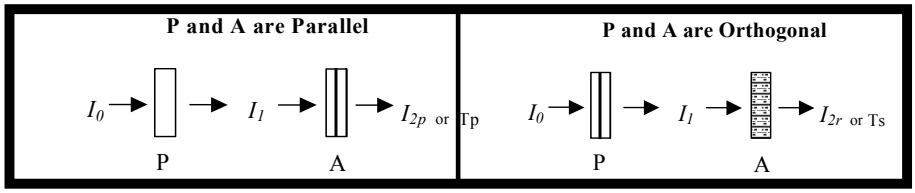

Figure 3-2 Cross polarization measurement setup

The extinction of polarizer P, in Figure 3-2, is

$R_P = \frac{I_{2p}}{I_z} \div \frac{I_{2_r}}{I_z}$, with $\frac{I_{2p}}{I_z}$ being the intensity of the desired transmission polarization (Tp) and with $\frac{I_{2_r}}{I_z}$ being the intensity of the rejected polarization (Ts) measured through the analyzer. In the orthogonal state, as shown in Figure 3-2, if polarizer P were to degrade, the intensity of Ts, measured through analyzer A, would increase proportional to the degradation of polarizer P.

3.2 Experimental Setup

When taking optical measurements with heat variations certain factors need to be considered. One such factor is optical beam expansion. Beam expansion is caused by index of refraction changes in the optical beam path. The index of refraction changes as a result of optical beam path interfaces having a different index from the transmitting medium. One example of this is the changing index of refraction between hot and cold air. Another example is the interface of air to glass. Because of optical beam expansion, light transmitted through the furnace is moving and shifting as a result of the changing refractive indices in the optical path. The experimental setup was chosen to increase the stability and accuracy of the detected optical signal.

Figure 3-3 shows the experimental setup of this research. A fiber optic cable transmits the light to a fiber optic collimating lens, which is mounted on a standard optical test bed. The collimated light is then transmitted into the furnace and through the test sample. After passing through the test sample, the light passes through the analyzer assembly. After the analyzer assembly the light enters an integrating sphere and is then transferred to the detector by way of another fiber optic cable.

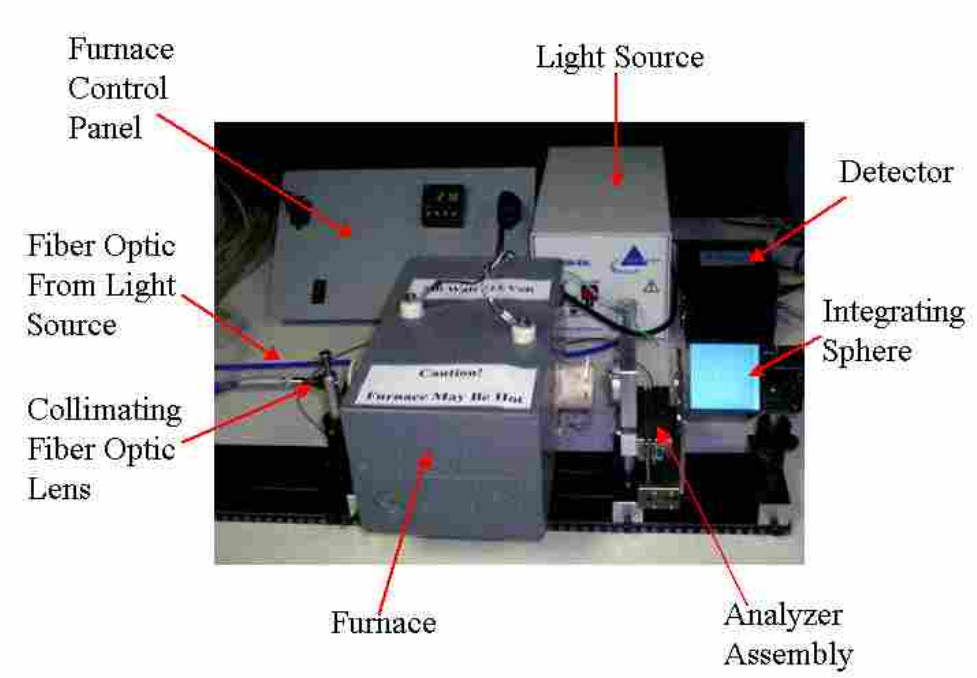

Figure 3-3 Experimental setup

3.2.1 Light Source

The light source used is a Mikropack DH-2000-BAL purchased from Ocean Optics. This light source was recommended by Ocean Optics as a highly stable light source, with less than 0.01% drift per hour (see Appendix A for complete light source

specifications), which could be used as part of an optical measurement tool. This light source requires a forty-minute warm-up time for maximum stability. The DH-2000-BAL source uses a combination of tungsten, deuterium, and halogen light sources to produce a balanced broad-spectrum stable light beam. Figure 3-4 is a representative picture of the light source used.

Figure 3-4 Mikropack DH-2000-BAL light source (picture courtesy of Ocean Optics)

3.2.2 Furnace

The furnace shown in Figure 3-3 is homemade. It was made by wrapping a 115-volt, 700-watt heating element around a ceramic tube. The ceramic tube is a high thermal conductivity ceramic with a 1-1/4 inch I.D. and a 1-1/2 inch O.D. The ceramic tube and element were encased with a high temperature refractory material inside of a metal enclosure. The heating element leads were then connected to the metal casing with ceramic bushings, shown in Figure 3-5.

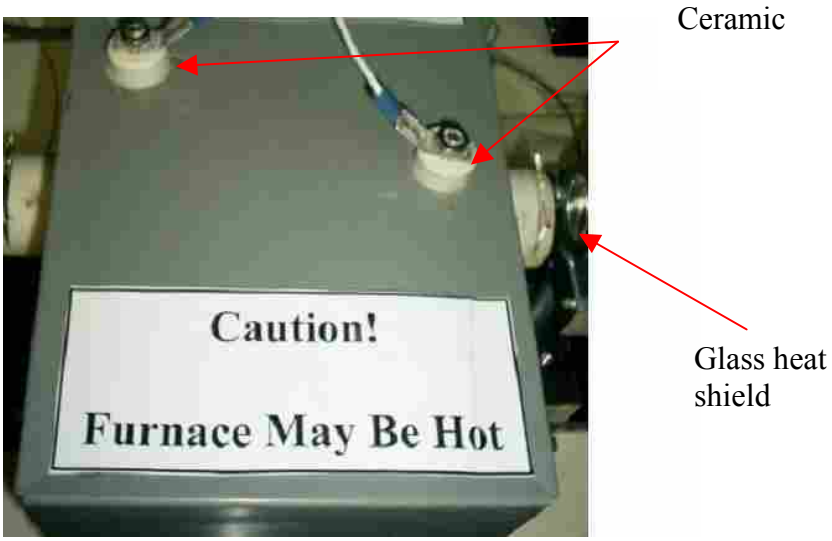

Figure 3-5 Homemade furnace

The ends of the ceramic tube extend about 1 inch on each side of the metal enclosure. Each ceramic tube end has a slot cut into the tube allowing a 1.4mm thick glass window to be installed as a heat shield. The windows help to maintain a stable temperature region within the tube, ± 3 ºC over a five-minute period. The furnace has been heated up to 700 ºC for the initial bake out process and to help cure the refractory material. Higher temperatures may be obtainable but have not been attempted.

3.2.3 Furnace Control

A standard temperature controller and a solid-state relay are used to control the furnace. Figure 3-6 is a block diagram of the furnace control setup.

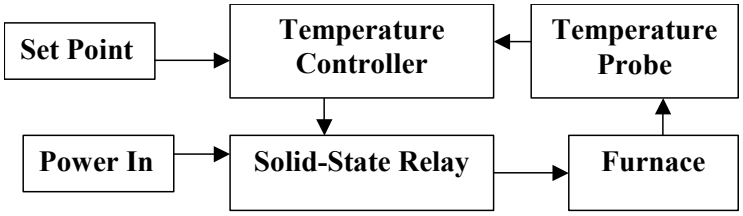

Figure 3-6 Furnace control block diagram

The temperature controller is an Omega Cni1644 with built-in cold junction compensation (see Appendix A for complete specifications). The temperature probe is a standard J-type thermocouple. The thermocouple probe is embedded in a cement mold with the tip of the thermocouple slightly protruding out of the top of the mold. The mold is positioned in the back half of the ceramic tube as shown in Figure 3-7.

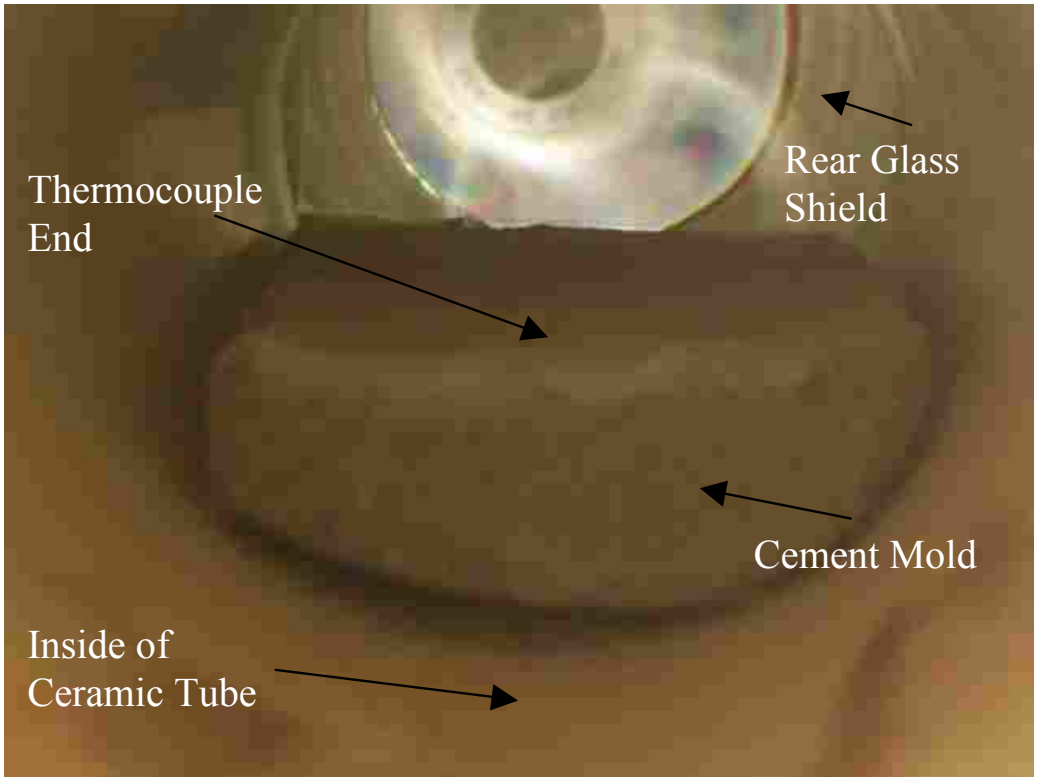

Figure 3-7 Temperature probe mold inside of ceramic tube

The mold is used to keep the thermocouple leads from shorting while also holding the thermocouple in a stable position near the center of the ceramic tube. The end of the thermocouple is on the top surface of the mold. Figure 3-8 shows the thermocouple leads and the cement mold positioned in the end of the ceramic tube. The cement mold and rear glass shield remained in a fixed position throughout the testing.

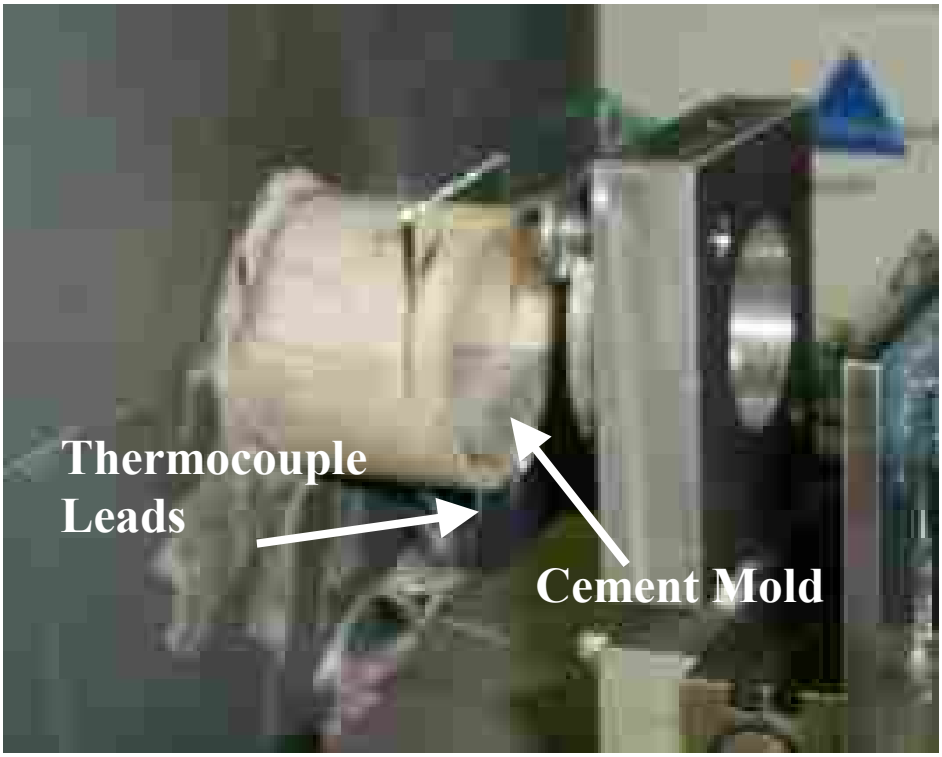

Figure 3-8 Exit side of furnace

3.2.4 Detector

The detector is an Ocean Optics QE65000 with an HC-1 grating option. This grating option allows the detector to work in the wavelength range from 200nm to 950nm. This detector was chosen because it is highly sensitive to light with a single intensity count being produced by 22 electrons for all wavelengths within its operational spectrum. In addition to its high sensitivity, the detector is precision cooled by a thermal electric module. Because of the controlled detector temperature, detector thermal drift and detector black noise is kept to a minimum (see Appendix A for complete detector and detector software specifications). See section 3.4 for detector drift and black noise data produced by the experimental setup. Figure 3-9 is a representative picture of the QE65000 spectrophotometer.

Figure 3-9 Ocean Optics QE65000 detector (picture courtesy of Ocean Optics)

The detector has programmable I/O for controlling the light source and other auxiliary functions. The software used is the standard Ocean Optics OOIbase32 software that comes with the detector. The OOIbase32 software has three user variables: integration time, boxcar smoothing, and sample averaging. The integration time is used to increase or decrease the signal to noise ratio. If the integration time is increased smaller signal levels can be more reliably detected. Boxcar smoothing is an adjustment that affects the position of the light compared to the position of the pixel or pixels. Sample averaging is the number of times a sample is averaged before outputting the detected average value. The optimal value for integration time was found to be 200ms, for boxcar smoothing 7, and for averaging 200 samples. All testing used these same values. These values were chosen because they gave the most reliable and repeatable results. The computer interface is USB and the optical interface is a fiber optic connection.

3.2.5 Integrating Sphere

The integrating sphere used is an Ocean Optics FOIS-1 as shown in Figure 3-10. This sphere was chosen because of the input aperture size and because of the fiber optic connection. This integrating sphere helps to smooth out the response of the effects of turbulent refraction caused by the heated air and allows the detector to function with increased precision.

Figure 3-10 FOIS-1 fiber optic integrating sphere (picture courtesy of Ocean Optics)

The input aperture of the integrating sphere is 9.5 mm, about ½ of the spot size of the incoming light beam.

3.2.6 Analyzer Assembly

The analyzer assembly, shown in Figure 3-11, consists of two WGP analyzers mounted on a slide assembly and a focusing lens mounted in the optical beam path. The slide assembly is used to move each analyzer independently into the optical beam path.

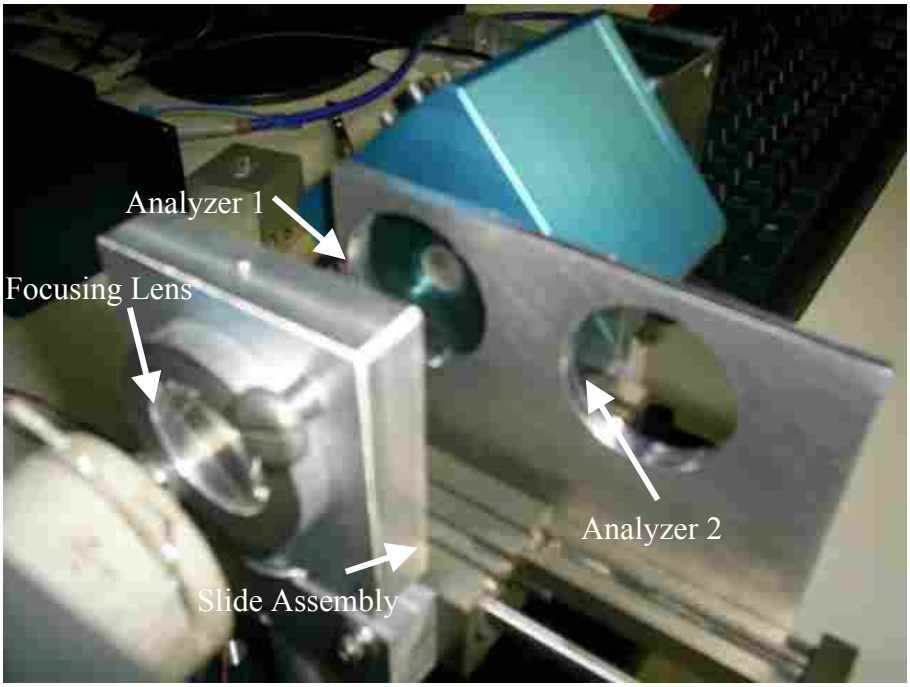

Figure 3-11 Analyzer assembly

3.2.6.1 WGP Analyzers

Each WGP analyzer is made from two high contrast WGPs mounted face to face. The transmission axes of the tandem WGPs are precision aligned for maximum transmission. When two WGPs are used in tandem the resulting transmission extinction is equal to the extinction of each polarizer multiplied together. For example, if two tandem WGPs each have an extinction of 1000, the resulting extinction is near 1000000. The analyzers used have extinctions greater than 1,000,000:1 for the 550nm wavelength. The polarizing wires of Analyzer 1 (Figure 3-11) are horizontal and orthogonal to the vertical polarizing wires of the fixed test sample. When taking the rejected-state polarization measurements, Analyzer 1 is positioned in the optical path as shown in Figure 3-11. Analyzer 2 is not used in this research, but is necessary if the extinction of the polarizer sample needed to be calculated.

3.2.7 Focusing Lens

In Figure 3-12, we are able to see the spot size of the light beam after passing through the focusing lens (the analyzer is shown in an intermediate non-standard position).

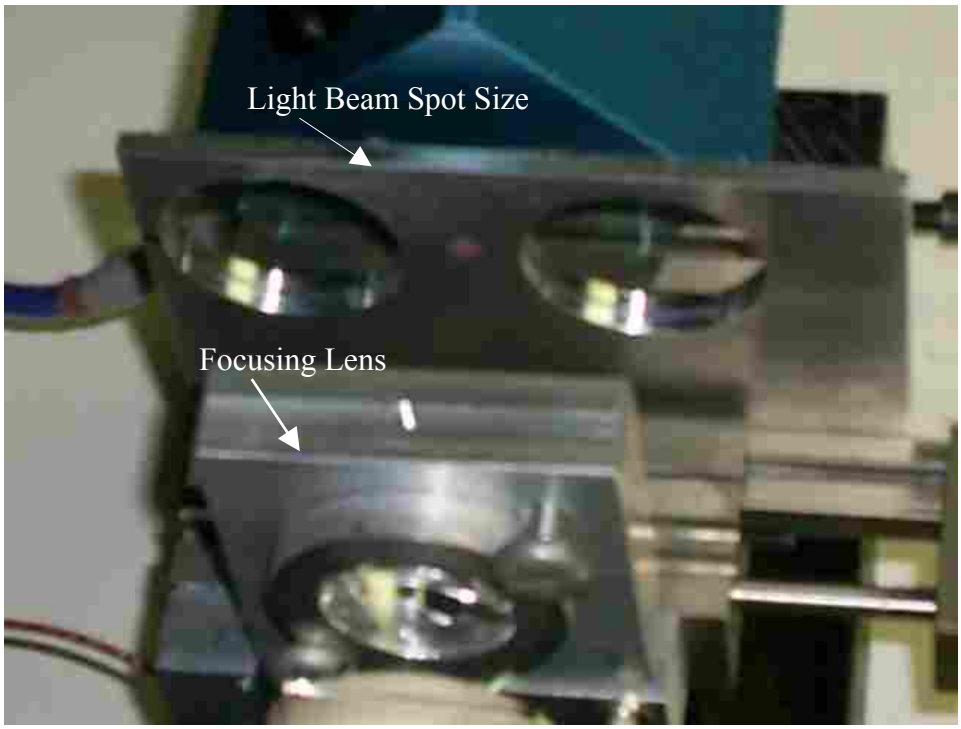

Figure 3-12 Analyzer assembly showing beam spot size

The focusing lens was needed to keep the spot size smaller than the input aperture of the integrating sphere. The lens was positioned so the focus of the light beam would be at the entrance face of the integrating sphere.

3.2.8 Samples

The WGP samples are a mushroom shape as shown in Figure 3-13. The flat part of the mushroom shape is oriented along the transmission axis of the WGP with the nano-

wires orthogonal to the flat cut. The samples are stored with the nano-wires facing upward for protection. The yellowish looking samples are samples that have been heat tested to the failure point.

Figure 3-13 Coated and uncoated test samples

A total of nine polarizer samples were tested, 3 magnesium fluoride over-coated, 3 silicon dioxide over-coated, and 3 uncoated.

3.2.9 Sample Holder

The sample holder is made from a 1-1/4 inch diameter stainless steel rod. The rod was milled down to a height of 8.8mm leaving it with a half-moon shape (see Figure 3-16). A shallow groove was then cut in the end of the sample holder to hold the stem of the mushroom shaped samples. Two screws were used to fasten a stainless steel end-cap to secure the sample (see Figure 3-14). The sample holder can be rotated while in the

ceramic tube for aligning the samples with the analyzers. Figure 3-15, shows a bare glass sample installed in the sample holder.

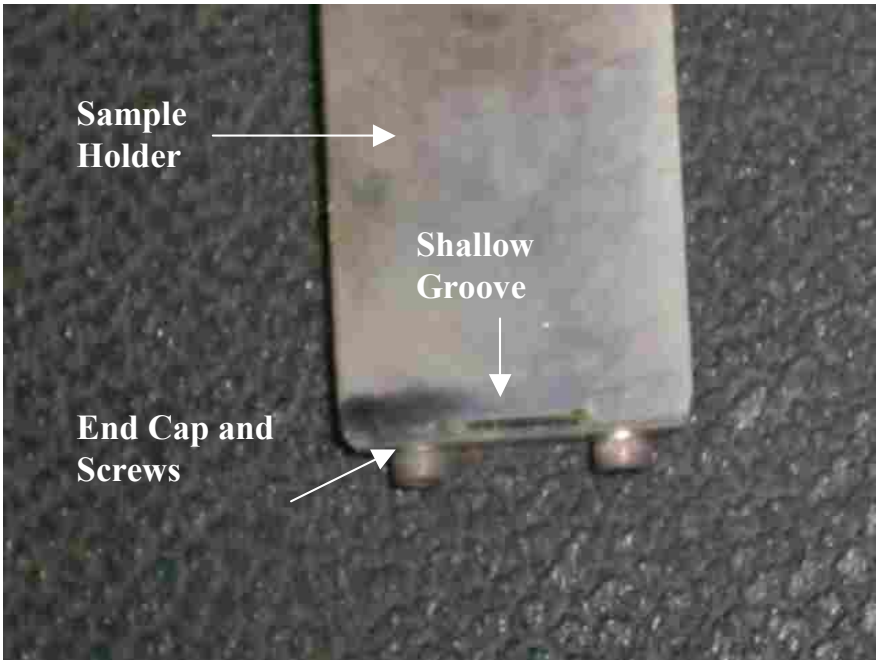

Figure 3-14 Sample holder (top view) without a sample installed

Figure 3-15 Sample holder with bare glass sample installed

With a sample installed, the sample and the sample holder form a circle. The circle is slightly smaller than the I.D. of the ceramic tube. The light beam spot size on the sample is shown in Figure 3-16. The light beam does not touch the ceramic tube as it passes through the furnace.

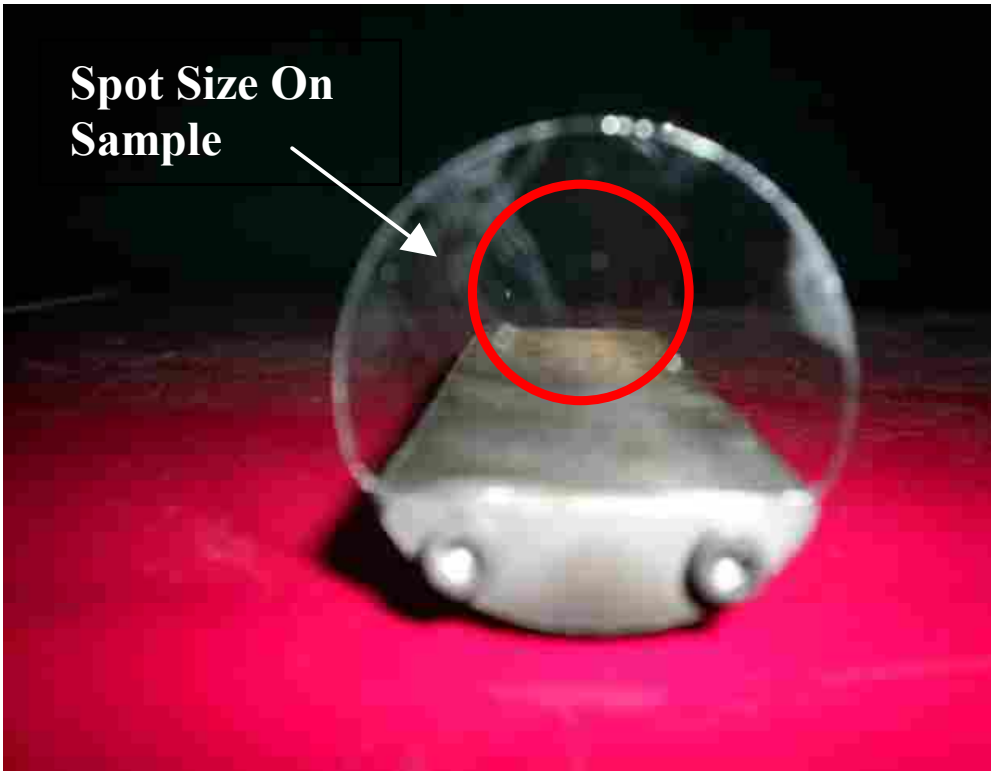

Figure 3-16 Light beam spot size

3.2.10 Sample Handling

When handling WGPs special precautions need to be taken to preserve the delicate nano-wires. Latex gloves should always be worn to keep oil from the finger from wicking into the nano-wires. Figure 3-17 is an example of oil wicking off of fingers and into the nano-wire structure. In Figure 3-17, we can see the oil migration happening from the bottom of the picture toward the top. The nano-wires create a strong capillary

force that readily draws in oil from the skin. The oil adds index of refraction changes to the WGP that negatively affects performance.

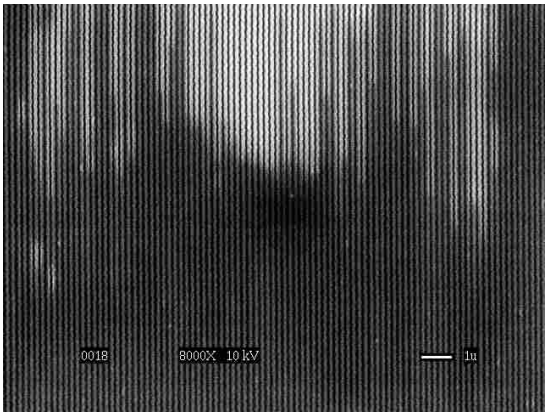

Figure 3-17 SEM of oil migration through the nano-wires (darker color is oil)

Figure 3-18 is an example of nano-wire damage due to mishandling. The SEM shows nano-wires that are toppled over and smashed together. This type of damage is caused by the nano-wire surface lightly brushing against a piece of cloth. The central dark vertical band and the two thinner bands on either side of the central one are caused by oil migration. Samples should be stored in a manor to prevent contact with the nano-wires.

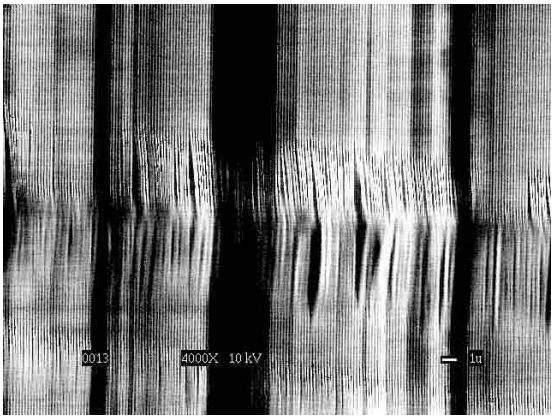

Figure 3-18 SEM of damaged nano-wires

3.3 Experimental Procedure

This procedure was repeated for each sample type at temperatures of 450 ºC, 500 ºC, and 550 ºC. The first step is to set the furnace to 450 ºC, turn on the light source, and turn on the thermal electric cooler on the detector. Wait 40 minutes for the furnace to reach equilibrium and for the detector and light source to stabilize. Then, with the sample holder installed inside of the furnace *without a sample* and with the heat shield glass windows placed in the ends of the ceramic tube and with the light source shuttered and all room lights turned off, take a background intensity reading I_z. Next, open the shutter and take the I_{oTs} measurement (with analyzer 1 in the light path). Next, while the furnace is still at temperature, remove the heat shield glass window at the entrance (use pliers or something that is heat resistant) and remove the sample holder from the furnace. Then, with latex gloves on, install the sample into the sample holder, with the wire side of the sample facing the detector, and replace the sample holder into the furnace. Replace the glass shield and move the light source mount post into the measurement position. Verify that the sample holder is aligned properly with the Alignment Marks on the ceramic tube (see Figure 3-19).

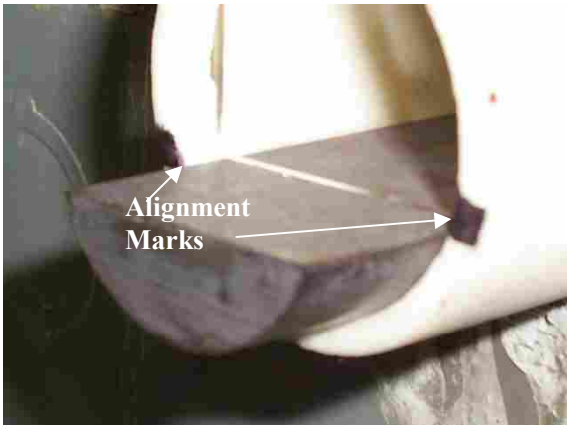

Figure 3-19 Alignment marks on ceramic tube

Immediately start the timed test for the Ts measurement. The Ts measurement represents s-state light leakage through the polarizer sample under test. The same procedure was then repeated for each temperature and sample tested, starting with a new background and I_{oTs} reading with the analyzer 1 in the light path.

3.4 Reliability Testing

Dark-state and bright-state reliability tests were conducted to determine the reliability of the experimental setup. All reliability testing was conducted with the furnace at 600 ºC without a sample installed and with an ambient temperature of 23.5 ± 2 ºC. Bright-state data is shown in Figure 3-20. The detector bright-state variations at 550nm were measured to have a standard deviation of .058551962% over a sixty-minute period. The bright-state light intensity was normalized to 100%, deviations from 100% are shown. The bright-state percent deviation represents light source variations and detector variations combined.

Dark-state data is shown in Figure 3-21. The intensity of the dark-state was normalized to zero and the resulting deviations from zero are shown for a sixty-minute time span. The detector variations at 550nm were measured to have a standard deviation of .056960951% over a sixty-minute period. The dark-state percent deviation represents variations in detector black noise and stray light variations incident upon the detector. The slope of the downward trend shown in Figure 3-21 represents detector drift.

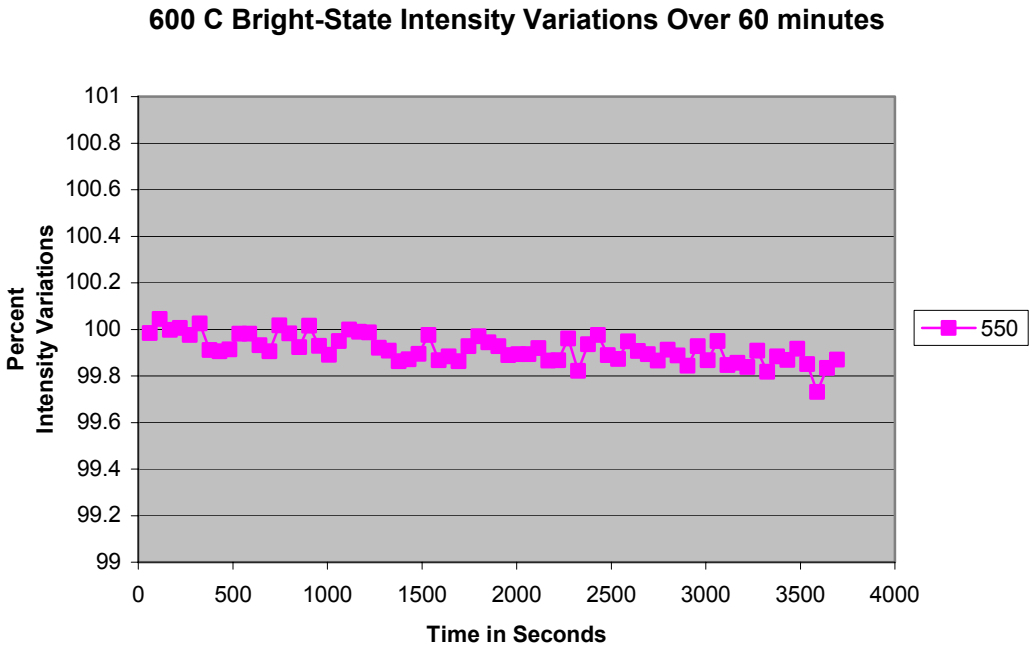

Figure 3-20 Bright-state variations at 550nm.

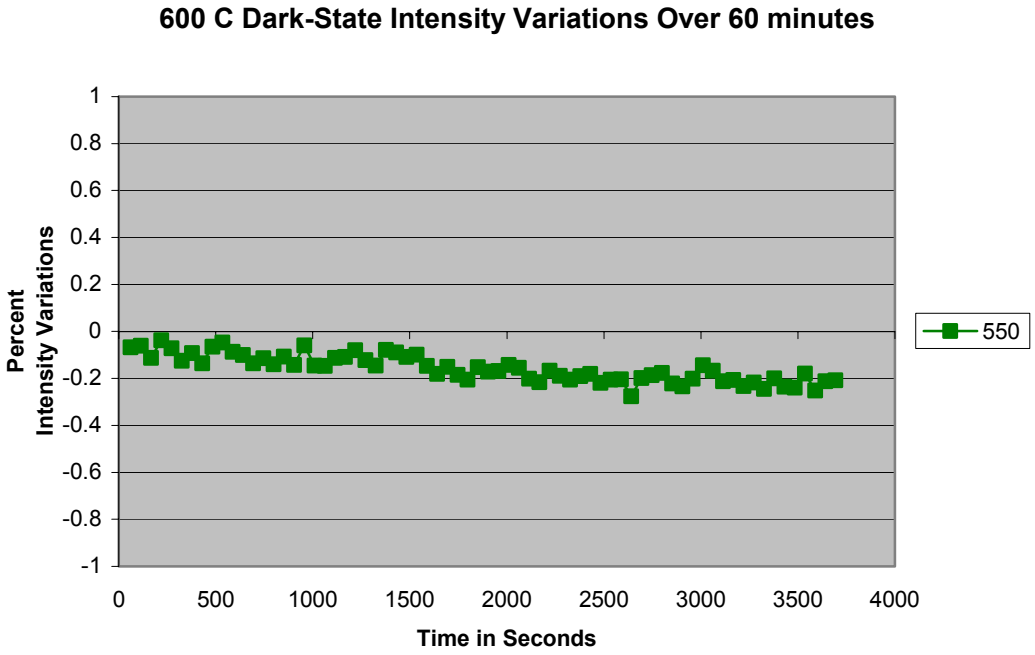

Figure 3-21 Dark-state variations at 550nm.

3.5 Repeatability Testing

In order to ascertain the measurement variability related to the sample fixture, eight iterations of mounting and dismounting the sample were performed. Each iteration consisted of removing the glass heat shield, removing the sample holder from the oven, removing and replacing the sample, reinstalling the sample holder, realigning the sample and taking a measurement. The results are shown in Figure 3-22. The greatest variation, contained in eight iterations, was found to be .069063%. This variation includes detector variability, light source variability, and misalignment variability all combined together.

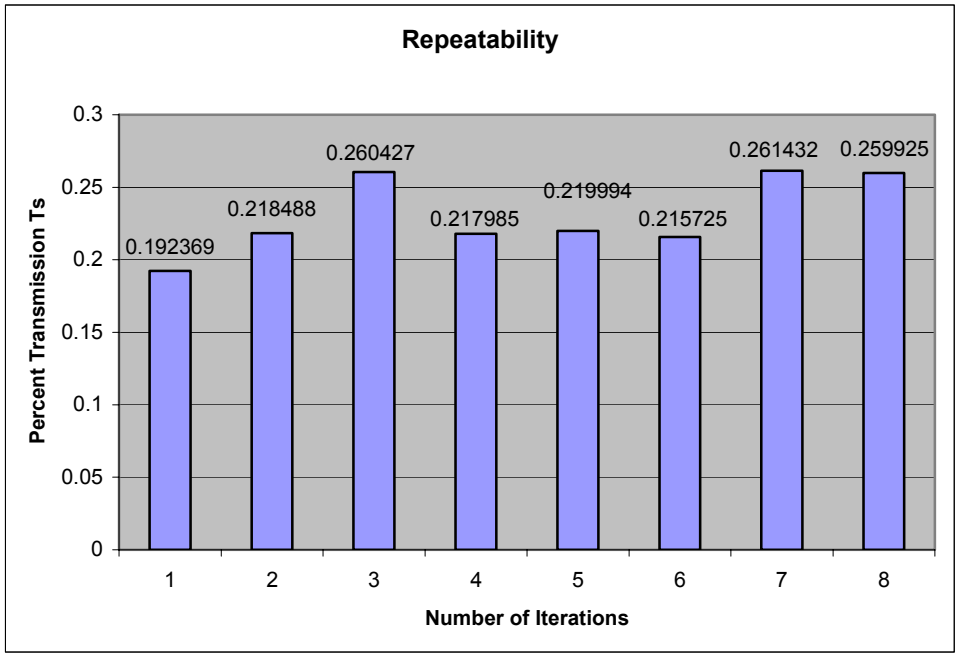

Figure 3-22 Repeatability of test fixture

3.6 Summary

An experimental setup was created to measure light intensities through a sample at temperatures of 450 ºC, 500 ºC, and 550 ºC while also tracking the time it took for the

light intensity to reach an s-state leakage of .8% measured through the test sample. The maximum variability of intensity readings produced by the experimental setup was found to be less than .1%. The test setup has been found to be robust and more than adequate to meet the analysis needs of this research. Test samples with over-coatings of magnesium fluoride, silicon dioxide and without any over-coatings were tested using the experimental setup. The next chapter will discuss the results of the testing in detail.

4 Data Analysis

4.1 No Over-coat

Figure 4-1 shows the results of the accelerated lifetime testing for WGPs with no protective over-coat. The red points represent failure data points. The green line in the middle represents the best-fit linear line and the green triangles represent the intersection of the test temperature with the best-fit linear line. The standard deviation of the natural logarithm of failure time was 0.1334. The broken-up lines are the upper and lower 90% confidence intervals for temperatures ranging from 723.15 Kelvin to 823.15 Kelvin (450°C to 550°C). Notice that the confidence intervals widen as the data is extrapolated in either direction. The activation energy was calculated to be 1.5329 eV. This activation is likely a combination of at least two failure modes: oxidation from the substrate to the aluminum nano-wires and oxidation from atmosphere to the aluminum nano-wires. The activation energy of a reaction resulting from source oxygen from the atmosphere is the lesser of the two.

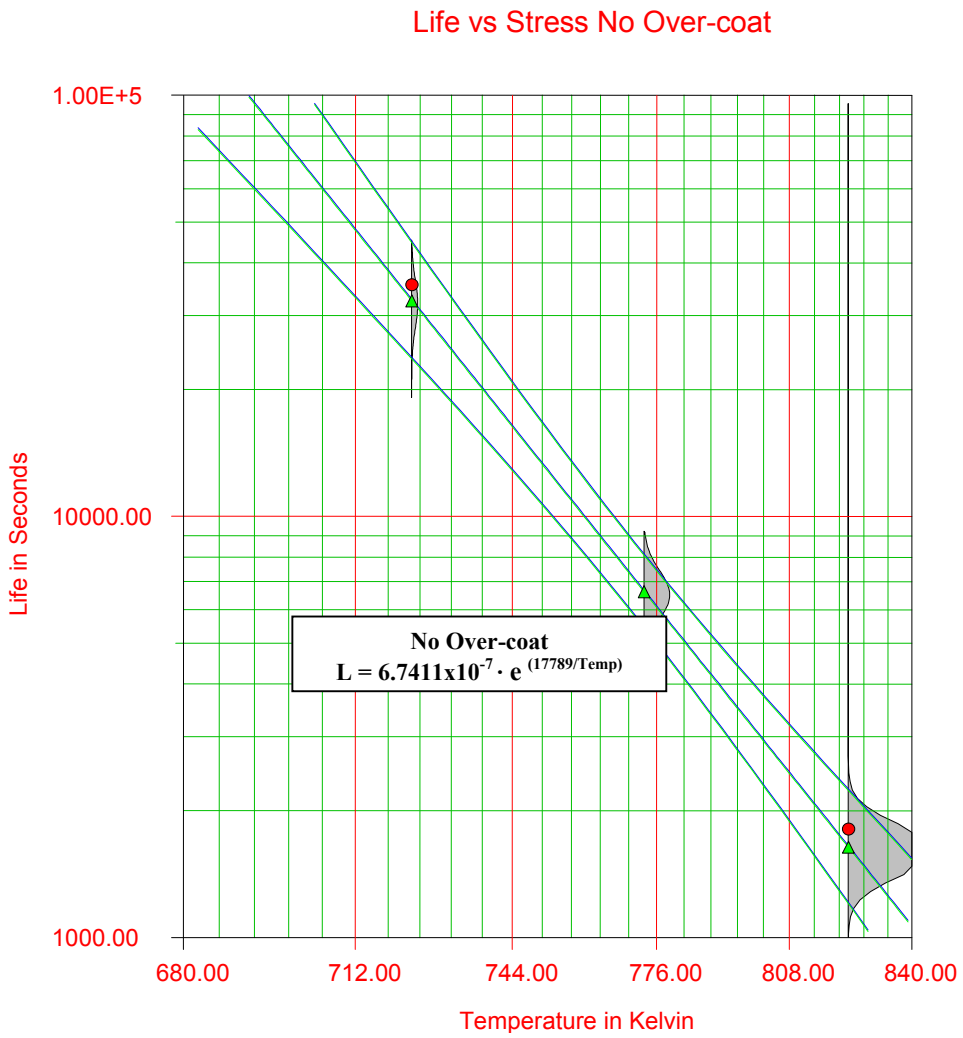

Figure 4-1 No over-coat accelerated testing results

4.1.1 SEM No Over-Coating

In Figure 4-2 we can see a difference in the texture between the aluminum nano-wires and the substrate. The aluminum wires are clearly exposed to atmosphere on the top and on both sides. Figure 4-3 is an SEM of a no over-coat WGP heat processed at 550 ºC for 1 hour. In Figure 4-3, the once aluminum wires are now completely aluminum oxide wires. Aluminum oxide is a very hard material with properties like ceramic.

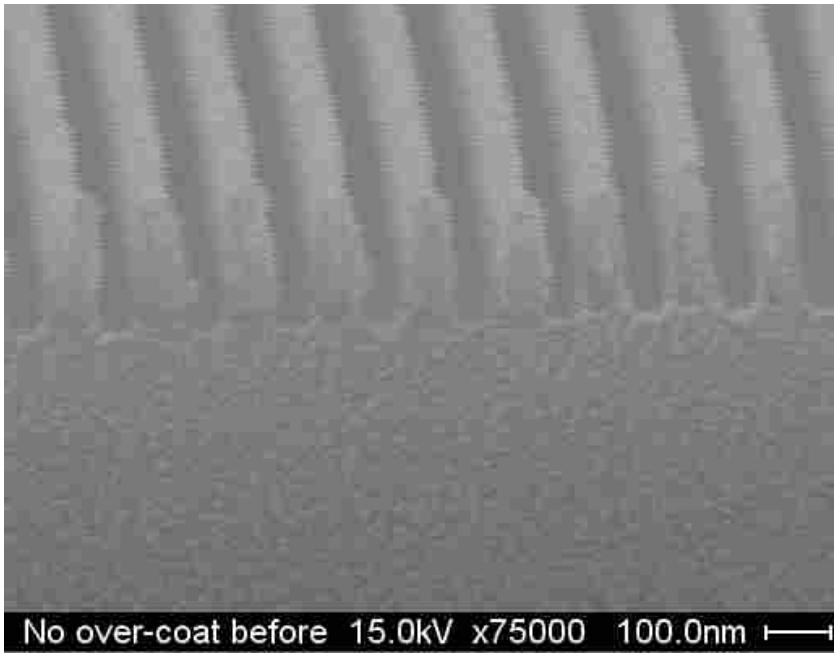

Figure 4-2 No over-coat before heat testing

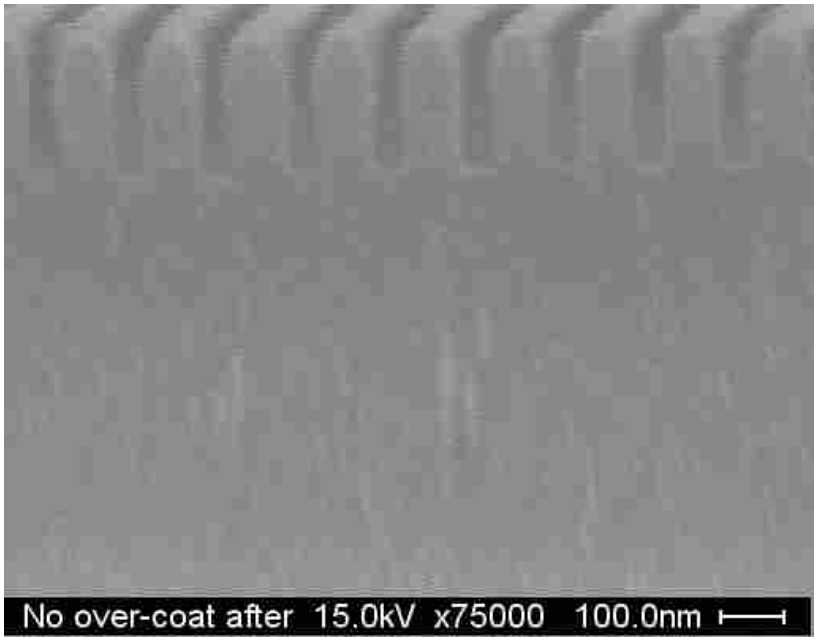

Figure 4-3 No over-coat after heat testing

As shown in Figure 4-4, the physical appearance of the polarizer before testing was a transparent grey and after heat testing it became a transparent brown color. The

color change suggests that the aluminum wires are no longer conductive and have changed into an aluminum oxide. The picture was taken at normal incidence and with no flash.

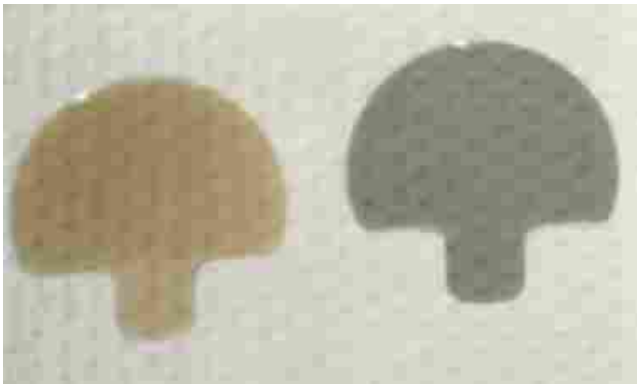

Figure 4-4 No over-coat WGPs after testing (left) and before testing (right)

4.2 Silicon Dioxide

Figure 4-5 shows the results of the lifetime testing of the silicon dioxide coated WGPs. The standard deviation of the natural logarithm of failure time was 0.0435. Notice that the confidence intervals are close together. This is a result of the data point being closer to the model Arrhenius fit. The activation energy was calculated to be 1.7197 eV. It is possible that the oxidation of WGPs with silicon dioxide over-coatings have three separate activation energies or failure modes: oxygen diffusing through the silicon dioxide on top of the aluminum nano-wires, oxygen diffusing from the substrate on the bottom of the aluminum nano-wires, and oxygen traveling through the gaps in the silicon dioxide layer above the troughs where the silicon dioxide failed to seal off the underlying wires completely (see Figure 4-6).

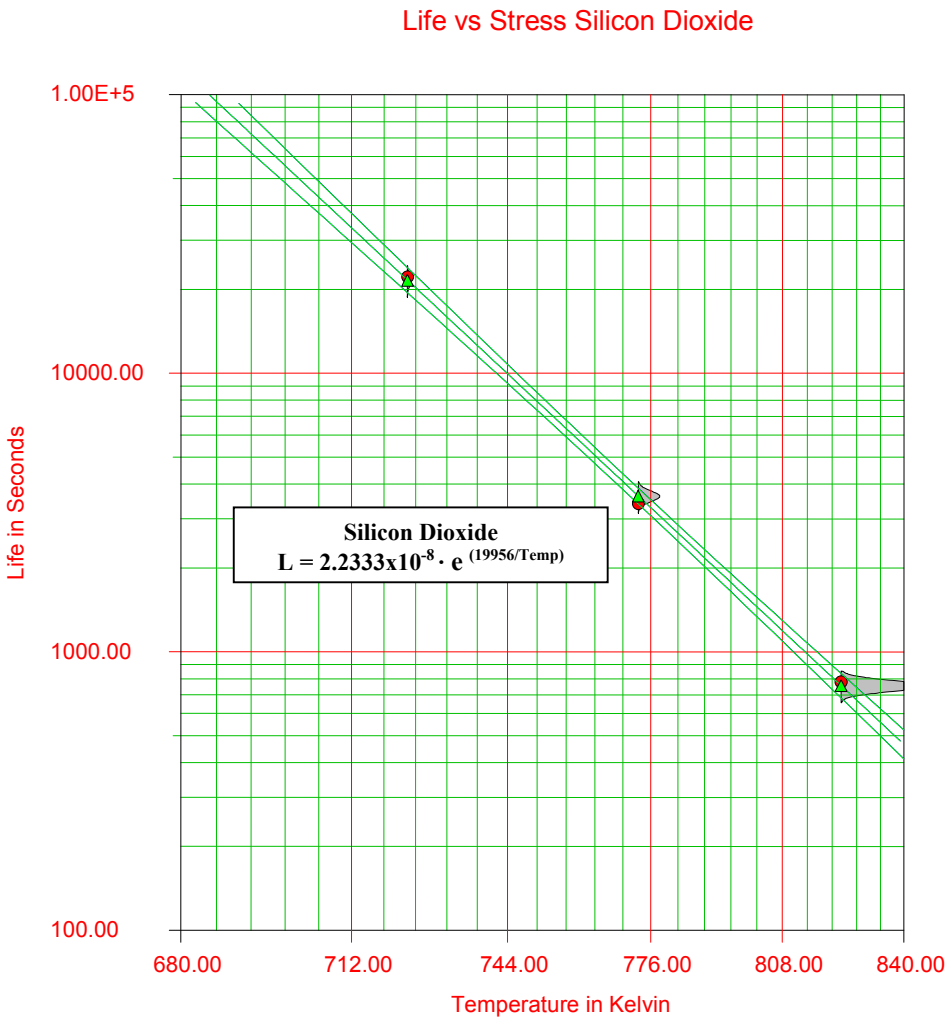

Figure 4-5 Silicon dioxide accelerated testing results

4.2.1 SEM Silicon Dioxide

Figure 4-6 is an SEM picture of a WGP with 100nm of silicon dioxide over-coating before it was heat tested. The bottom half of the SEM is the glass substrate, mostly comprising silicon and oxygen. On the substrate are aluminum wires over-coated with silicon dioxide. It can be seen that each wire is coated with a consistent coating of silicon dioxide.

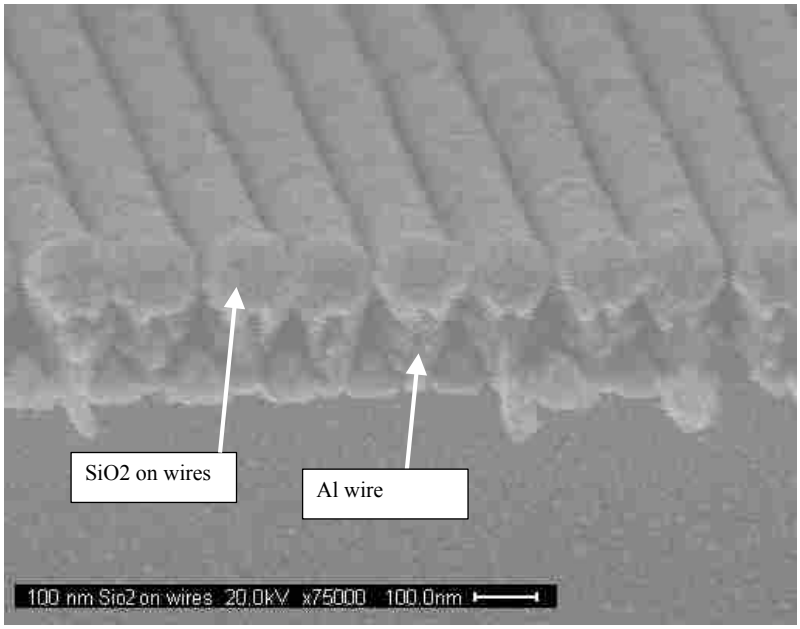

Figure 4-6 Silicon dioxide over-coated before heat testing

Figure 4-7 is an SEM of a silicon dioxide over-coated WGP heat processed at 550 ºC for 1 hour. It appears that the whole structure has oxidized together. The silicon dioxide over-coating, aluminum oxide wires, and the substrate all seem to have joined together into a single physical oxide bond.

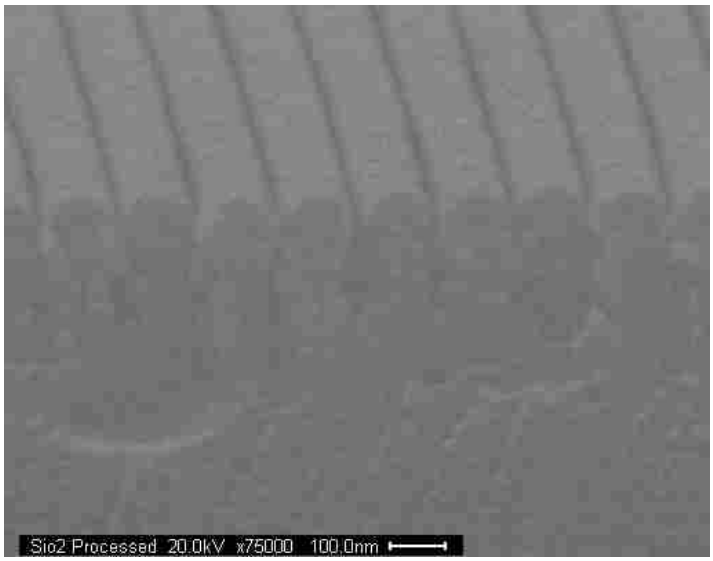

Figure 4-7 SiO_2 after heat testing

Before heat testing the silicon dioxide over-coated WGP, it had an aluminum appearance as shown in Figure 4-8. After heat testing the appearance changed from a reflective metal color to a transparent yellow color. Again, the color change suggests that the aluminum has turned into a clear oxide. The picture was taken at normal incidence with the flash on.

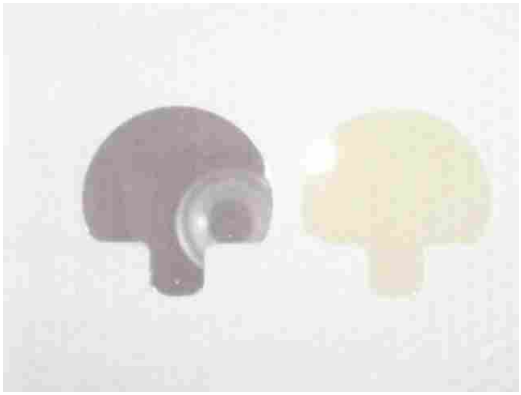

Figure 4-8 Silicon dioxide before testing (left) and after testing (right)

4.3 Magnesium Fluoride

Figure 4-9 shows the results of accelerated testing of WGPs with a magnesium fluoride protective layer. The standard deviation of the natural logarithm of failure time was 0.1559.. The activation energy was calculated to be 2.4577 eV. The oxidation of WGPs with magnesium fluoride over-coating has, at least, two likely activation energies; one activation energy resulting from oxygen diffusion from the substrate and the other from oxygen migration through gaps in the coating layer over the troughs similar to those in the silicon dioxide coating (see Figure 4-10). Unlike the silicon dioxide over-coating, the magnesium fluoride layer does not constitute a significant source of oxygen for oxygen diffusion through the magnesium fluoride itself.

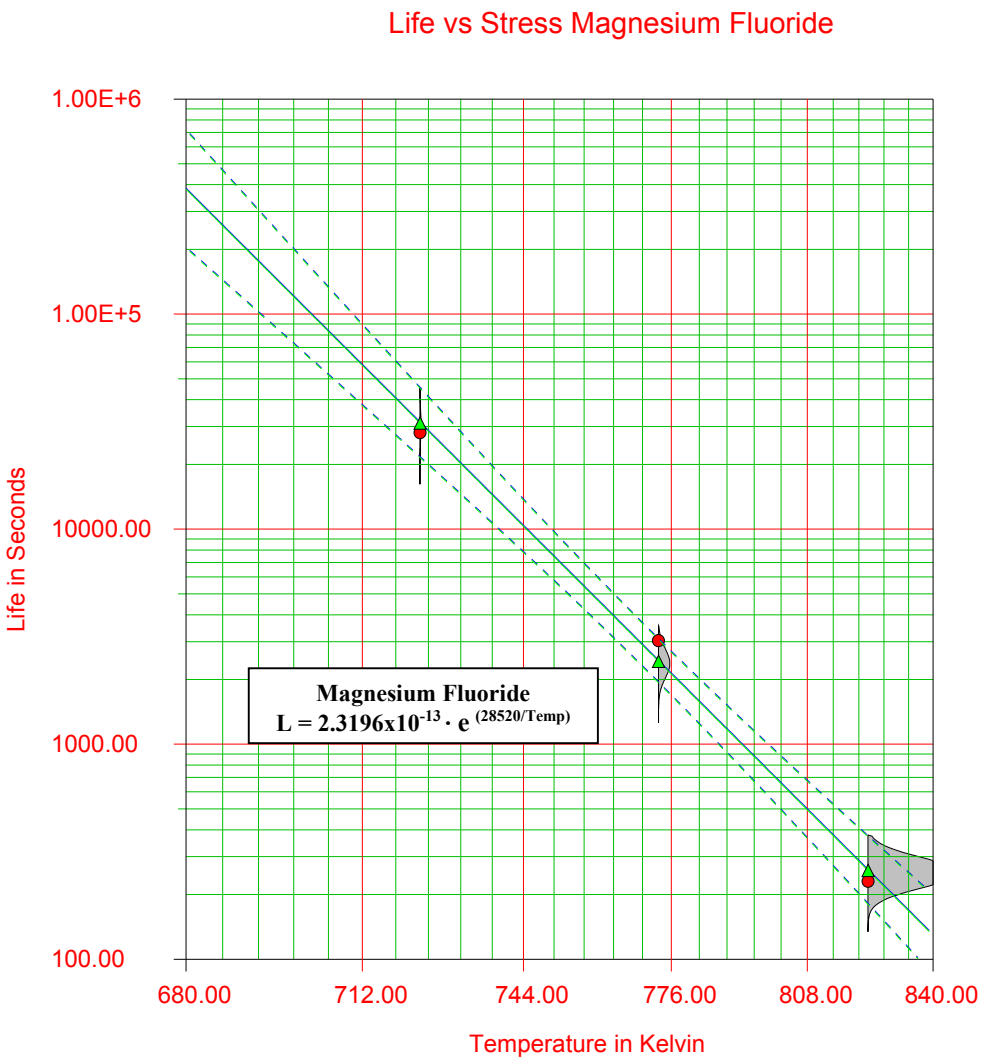

Figure 4-9 Magnesium fluoride accelerated testing results

4.3.1 SEM Magnesium Fluoride

Figure 4-10 is an SEM picture of a WGP with 300nm of magnesium fluoride over-coating before it was heat tested. The bottom half of the SEM is the glass substrate, mostly comprising silicon and oxygen. On the substrate are aluminum wires over-coated with magnesium fluoride. It can be seen that each wire is coated with a consistent coating of magnesium fluoride.

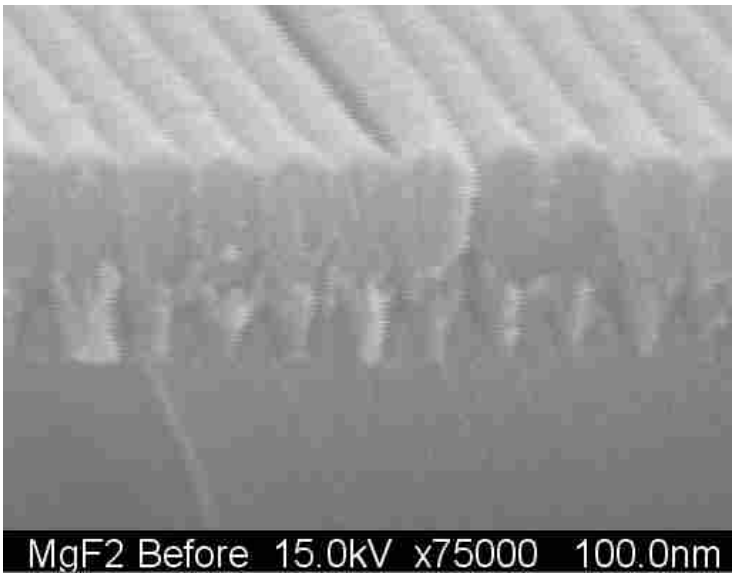

Figure 4-10 MgF_2 over-coated before heat testing

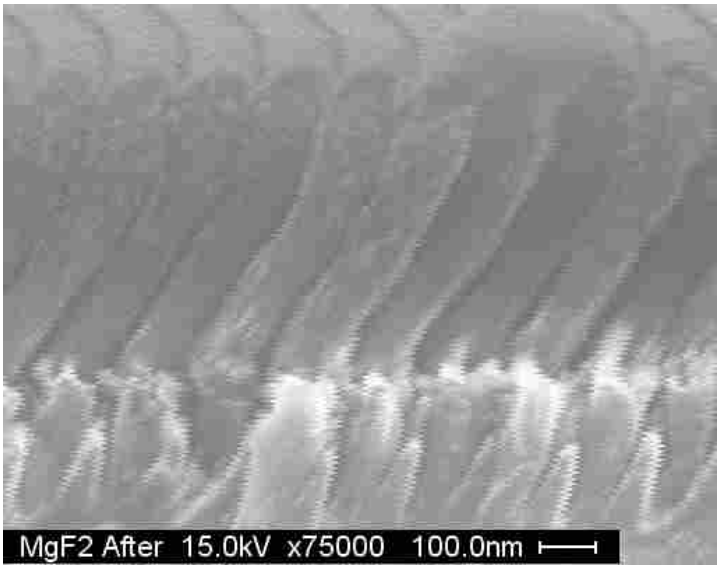

Figure 4-11 MgF_2 over-coated after heat testing

Figure 4-11 is an SEM of a magnesium fluoride over-coated WGP heat processed at 550 ºC for 1 hour. Close examination of the photo shows that the oxidation has mostly come upward from the substrate. This is evidenced by the triangular shaped wedges coming up between the nano-wires. The top of the magnesium fluoride over-coating

appears to be smashed together thus providing a good passivation layer, both before and after testing. In Figure 4-11 the MgF_2 is slanted to the right. This is believed to be because of the oxide growth from beneath the MgF_2.

Before heat testing the magnesium fluoride over-coated WGP, had a reflective appearance when viewed from an angle (shown in Figure 4-12). The picture was taken with bright light directly reflecting off of the surface of the polarizer toward the camera, with the flash off, and at an angle of about 45º from light source to polarizer and camera to polarizer. After heat testing the appearance changed to a reflective purple color when viewed from an angle (see Figure 4-12). The color change shows that the reflectivity of the magnesium fluoride sample is decreased with heat treatment. This is consistent with the underlying aluminum having been changed into an oxide.

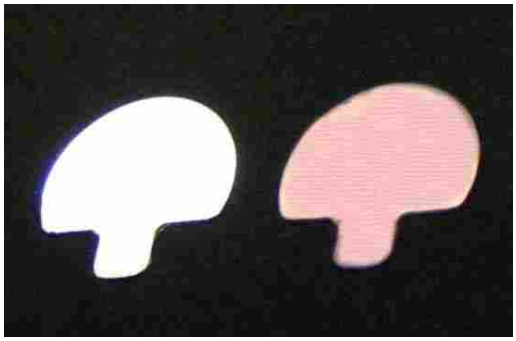

Figure 4-12 Magnesium fluoride before heat testing (left) and after heat testing (right)

4.4 Comparison of SiO_2, MgF_2, and No Over-coat Samples

In the Arrhenius plot shown in Figure 4-13, the y-axis represents the natural logarithm of the time to failure of the samples and the x-axis represents the inverse temperature in Kelvins. As temperature increases the failure time decreases. A best-fit

linear line was drawn through the failure points of each coating type. The magnesium fluoride has the greatest slope. This means that less change occurs in the samples coated with magnesium fluoride, in a given amount of time, compared to silicon dioxide and no over-coat; the length of the line is shorter in given time period. It can be easily seen that the magnesium fluoride samples exhibit the greatest resistance to heat. The silicon dioxide samples are next, and then the samples with no over-coat. The silicon dioxide samples and the no over-coat samples have similar slopes. The slope of the line is the activation energy of the chemical reaction; the greater the slope the higher the activation energy.

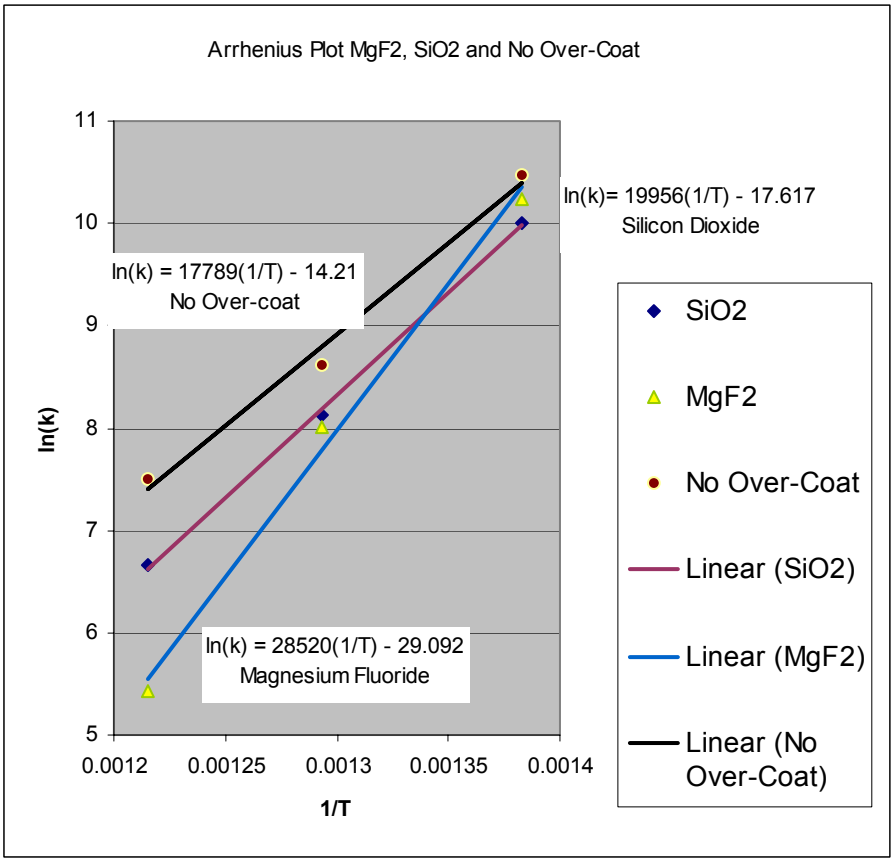

Figure 4-13 Arrhenius plots of SiO_2, MgF_2 and no over-coat samples

Figure 4-14 shows a summary of the actual data collected for each over-coating type. The data shows that the relationship between temperature and failure is a log-linear relationship, and that the data fits the Arrhenius equation very nicely. Additional data and graphs can be found in Appendix B.

No Over-coating	Temp (K)	k (seconds)	ln(k)	1/T
450 C	723.15	35500	10.47729	0.001383
500 C	773.15	5485	8.609772	0.001293
550 C	823.15	1810	7.501082	0.001215
Magnesium Fluoride Over-coating				
450 C	723.15	28100	10.24352	0.001383
500 C	773.15	3030	8.016318	0.001293
550 C	823.15	230	5.438079	0.001215
Silicon Dioxide Over-coating				
450 C	723.15	22200	10.00785	0.001383
500 C	773.15	3405	8.133	0.001293
550 C	823.15	780	6.659294	0.001215

Figure 4-14 Combined failure data of each over-coating

Figure 4-15 shows the extrapolated Arrhenius lifetime vs temperature plots for magnesium fluoride, silicon dioxide, and no over-coated WGPs. This lifetime extrapolation should be a modest lifetime estimate of WGP failures due to aluminum oxidation.

The data points measured for this research are shown in Figure 4-15 at 723.15 K, 773.15 K, and 823.15 K. Extrapolating the Arrhenius equations that fit each of these lines gives us the three lines shown in this figure. Magnesium fluoride shows a clear lifetime advantage compared to silicon dioxide and no over-coating.

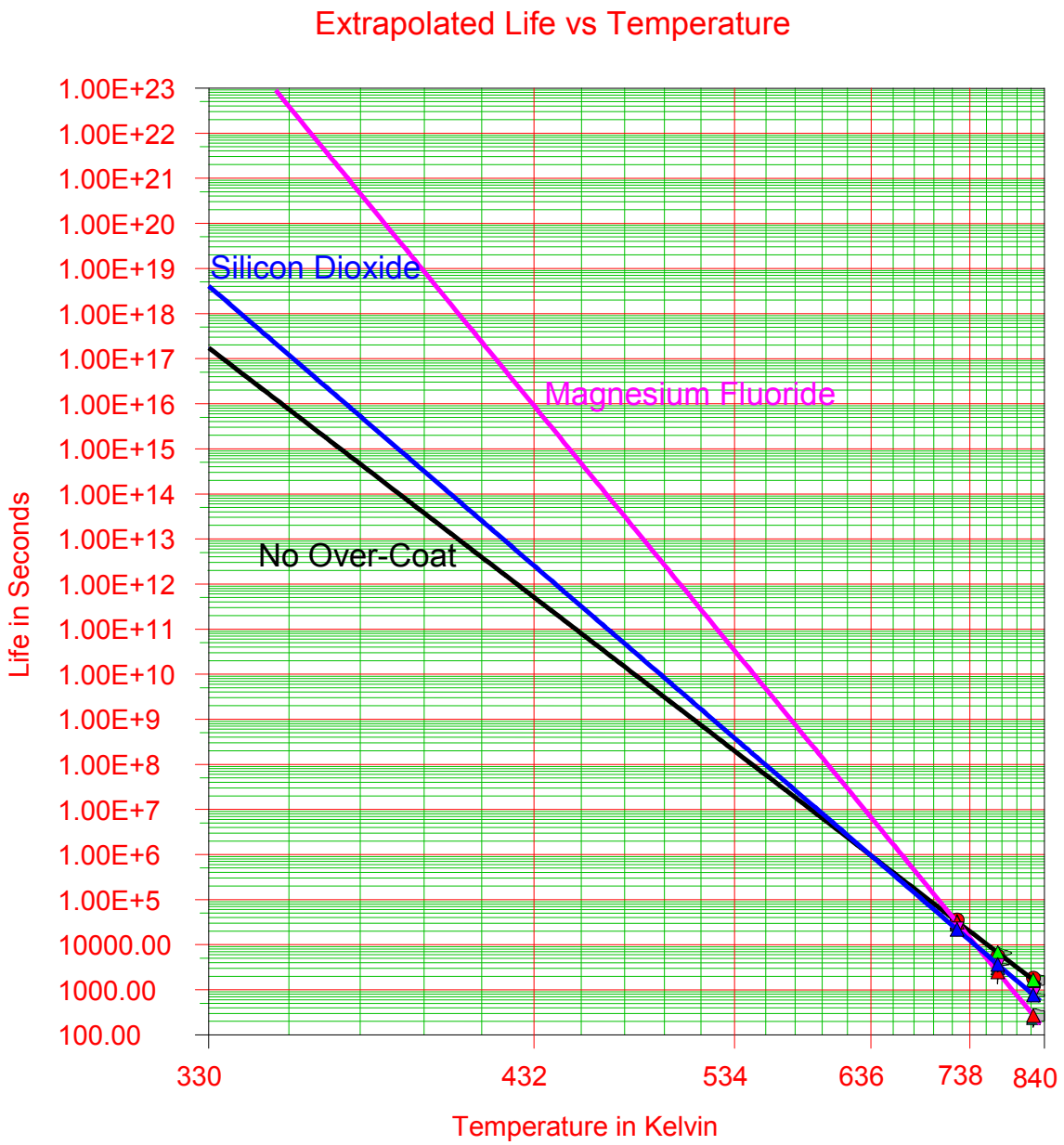

Figure 4-15 Extrapolated lifetime data of all sample types

4.5 Summary

Failure points for three WGPs have been analyzed using the Arrhenius life stress model. Analyzing SEM pictures and deducing possible paths through which oxygen could reach the aluminum wires have revealed likely failure modes. Magnesium fluoride

was found to have the highest activation energy and therefore the best heat resistance. Beyond oxidation, no parasitic degradation was found to be present with accelerated heat testing of magnesium fluoride or silicon dioxide over-coatings.

High temperature applications of WGPs call for their ambient temperature to be between 150 ºC and 250 °C. Based on the findings shown in Figure 4-15, at 250 ºC, the MgF_2-coated WGPs would last 1.1 X 10^{11} seconds (3,488 years), the SiO_2-coated WGPs would last 8.2315 X 10^8 seconds (26.1 years), and the WGPs with no over-coating would last 3.9475 X 10^8 seconds (12.5 years). This means that a SiO_2 over-coating provides a lifetime improvement of 208%, and a MgF_2 over-coating provides a lifetime improvement of 27,904%.

5 Conclusions and Recommendations

5.1 Research Summary

Wire-grid polarizers (WGPs) are constructed of periodic parallel conductive wires. Normally, such a structure would function as a simple diffraction grating, but when the pitch or period of the wires is less than about half the wavelength of the incoming light, it becomes a polarizer. The first wire-grid polarizers were invented in the late 1800's. by Hertz. These polarizers polarized radio waves and had relatively large periods. Recently, the period of the wires has been reduced enough to enable their use in the visible spectrum.

Visible spectrum wire-grid polarizers have periods measured in nanometers. In order to achieve nanometer-sized periods, the wire, usually made of aluminum, needs to be on the nano-scale also. Aluminum nano-wires are fragile; any slight contact will destroy them, so it would be desirable to find a way to protect these fragile wires. Overcoating is one way this could be done.

Visible spectrum wire-grid polarizers have been found to have many diverse applications. Some of the applications require the WGPs to be exposed to high temperatures. Unlike traditional polymer polarizers, wire-grid polarizers are highly resistant to heat because they are made entirely of inorganic materials. Because of their

heat resistance, they are being designed into high temperature polarization applications such as high lumen lighting, laser applications, high lumen cinema projectors, and LED packaging.

Over-coatings for the WGP are necessary for creating a planarization layer and for providing protection for the delicate nano-wires. Planarization is desirable to allow the WGP to be easily integrated with other optical components. The protective coating makes handling and cleaning WGPs easier. Despite the new popularity of WGPs, lifetime data related to coated or uncoated WGPs has not been available, and questions about whether the coatings would in some way damage the aluminum nano-wires have remained unanswered.

Because WGP degradation failures do not occur under normal stress conditions within a reasonable amount of time, accelerated heat testing is needed to produce premature failures. Accelerated heat testing is commonly used in the semiconductor and electro-optical industries to determine product failure modes and to predict product lifetimes. In particular, Yang et al, used constant accelerated heat testing along with the Arrhenius model to predict lifetimes of optical transmitters. (Yang) Following these well established procedures, this research applies accelerated heat testing to a new area, optical wire-grid polarizers and uses it to document and compare failure modes and lifetime estimates of WGPs with coatings of magnesium fluoride, silicon dioxide, and WGPs without any coatings.

Since this is the first time WGPs have been tested this way, equipment for monitoring the optical properties of a sample while it is inside a highly controlled oven were not available. A special ceramic oven with optical ports was constructed to allow

the in situ optical monitoring while applying constant, uninterrupted heat to the test samples. Keeping the light spot size of the beam small as it entered the test chamber and capturing all transmitted light with an integrating sphere on the other end accounted for refractive problems associated with the heat of the furnace. WGPs with over-coatings of magnesium fluoride, silicon dioxide and WGPS without any over-coating were then heated in the oven, and input and output intensities were measured at temperatures of 450 ºC, 500 ºC, and 550 ºC while also tracking the time it took for the light intensity to reach an s-state leakage of 0.8%. The maximum variability of intensity readings produced by the experimental setup was found to be less than 0.1%. The test setup was found to be robust and more than adequate to meet the analysis needs of this research.

Optical observations and SEMs of the failed polarizers showed that the main failure mode was that of oxygen combining with the aluminum ribs to form the transparent aluminum oxide. Aluminum oxide seemed to form more readily in samples with an apparent source of oxygen.

Activation energies, the energy needed to cause a failure reaction in the sample, were calculated by applying the Arrhenius model to the failure data. WGPs with no over-coating were found to have an activation energy $\geq$ 1.5329 eV, with silicon dioxide an activation energy $\geq$ 1.7197 eV, and with magnesium fluoride an activation energy $\geq$ 2.4577 eV.

In doing this research, it was discovered that coating a WGP with an over-coating of silicon dioxide or magnesium fluoride slows the oxidation process of the aluminum nano-wires, thus increasing the lifetime of the WGP by 208% and an incredible 27,904%, respectively. Parasitic chemical reactions were not found to exist with silicon dioxide or

magnesium fluoride when used as an over-coating. Thus, the over-coatings not only protect the nano-wires from mechanical shock, which was a prime purpose for their usage, but as this study shows, they are extremely effective in protecting the aluminum wires from environmental oxidation reactions.

The lifetime of WGPs used in high temperature applications, such as high power polarized lighting, high lumen video projectors, or in polarized light recycling devices, has been shown by this research to be lengthened if magnesium fluoride or silicon dioxide is used as an over-coating.

5.2 Conclusions

This research shows that lifetime testing of WGPs can be conducted in a highly repeatable, carefully controlled environment. The question of whether over-coatings of magnesium fluoride or silicon dioxide would damage the aluminum wires on wire-grid polarizers has also been answered. The research has soundly rejected the null hypothesis, i.e., the statement "over-coatings will not affect the lifetime of the aluminum wires" has been proven to be wrong. Over-coatings of magnesium fluoride or of silicon dioxide significantly improve the lifetimes.

This research serves as a starting point for further work in accelerated lifetime testing of WGPs and in finding optimal over-coatings for physically protecting them and for prolonging their lifetimes.

5.3 Recommendations For Future Research

The WGPs tested in the research were limited to a 300 nm over-coating of magnesium fluoride and a 100 nm over-coating of silicon dioxide. Questions that were not addressed in this research, but which are certainly worth pursuing, would include the following:

1) Is the oxygen passivation effect of the over-coatings tied to the thickness of the over-coating?

2) Will the activation energy change with differing thicknesses of over-coat material?

3) It was observed that the extreme exposure to heat converted the aluminum nano-wires into an all-dielectric material. The resulting dielectric nano-wires were extremely hard like a ceramic. This hard material could have possible applications in chemical processing, nano-wire extruding, hydrophobic surface tension reduction, bearing manufacture, injection molding, nano-polishing, etc. The all-dielectric material also has a high dielectric strength. Other possible applications that might benefit from dielectric strength properties may include capacitors, resistors, nano-insulators, etc.

4) Can aluminum nano-wires be used as a thermal fuse?

5) How does the resistance of aluminum wires change with oxidation of the wire?

6) Can partial oxidation of the nano-wire serve a useful purpose in optimizing and designing integrated optics?

7) As the wires change from a metal to a dielectric, is optical phase retardance added to the WGP?

All these questions pose useful areas for further research.

Bibliography

Aubel, O.; Hasse, W.; Hommel, M. (2003) "Highly accelerated electromigration lifetime test (HALT) of copper" Device and Materials Reliability, IEEE Transactions on Volume 3, Issue 4, Dec. 2003 Page(s):213 - 217

Bird, G. R., and Parrish, Jr., M. (1960) "The wire grid as a near-infrared polarizer." J. Opt. Soc. Am. Vol. 50, pp. 886-891.

Hansen, D. P., and Gunther, J. E. (1998) "Polarizer Apparatus For Producing A Generally Polarized Beam of Light" U.S. Patent 6,108,131

Hertz, H., (1893). "Electric Waves" Macmillan and Company, Ltd., London, pp. 177.

Kahn, F. J., (2001). "Focus: Doing it with stripes" Private Line Report, Kahn International, 7(10).

Kostel, H., (2003). " Changing the Rules For Optical System Design" NanoOpto white paper. http://www.nanoopto.com/pdfs/nanoopto_wp_2003_june.pdf

Kurtz, A. F., Silverstein, B. D., and Mi, X. D. (2005). "SPATIALLY PATTERNED POLARIZATION COMPENSATOR" U.S. Patent 7,023,512

Lall, P., (2004). "Challenges in accelerated life testing" Thermal and Thermomechanical Phenomena in Electronic Systems, Volume 2, 1-4 June 2004 Page(s):727 Vol.2

Manca, J.V. Wondrak, W.; Croes, K.; De Ceuninck, W.; D'Haeger, V.; De Schepper, L.; Tielemans, L. (1999) "The Arrhenius relation for electronics in extreme temperature conditions" High Temperature Electronics, Page(s):29 - 32

Meeker, W.Q., Escobar, L.A. (1998) "Pitfalls of accelerated testing" Reliability, IEEE Transactions on Volume 47, Issue 2, Page(s):114 – 118

Moxtek (2002). "Polarization Measurement" Moxtek white paper http://moxtek.com/uploads/POLARIZATION_MEASUREMENT.pdf

Nelson, W.B. (2005) "A bibliography of accelerated test plans" Reliability, IEEE Transactions on Volume 54, Issue 2, June 2005 Page(s):194 - 197

Perkins, R. T., Hansen, D. P., Gardner, E. W., Thorne, J. M., and Robbins, A. A. (2000) "Broadband Wire Grid Polarizer for the Visible Spectrum" U.S. Patent 6,122,103

Polcawich, R.G., Feng, C., Vanatta, P., Piekarz, R., Trolier-McKinstry, S., Dubey, M., Ervin, M. (2000) "Highly accelerated lifetime testing (HALT) of lead zirconate titanate (PZT) thin films" Applications of Ferroelectrics, 2000. ISAF 2000. Proceedings of the 2000 12th IEEE International Symposium on Volume 1, 21 July-2 Aug. 2000 Page(s):357 - 360 vol. 1

Proflux (2004). "Polarizers and Polarizing Beam Splitters" Moxtek white paper http://moxtek.com/uploads/GENERAL_PURPOSE_POLARIZING_BEAMSPLITTERS.pdf

Wang, J. J., Zhang, W., Deng, Z., Deng, J., Liu, F., Sciortino, P., and Chen, L. (2005) "High-performance large-area ultra-broadband nanowire-grid polarizers and polarizing beam-splitters" Proc., SPIE Vol 5931, 59310D.

Yang, C., Liu, T., Xiang, C., and Ye, J., "Lifetime Test for Optical Transmitters in the ATLAS Liquid Argon Calorimeter Readout System" Physics Department SMU, Dallas Texas. http://www.physics.smu.edu/~scalise/SMUpreprints/SMU-HEP-05-13.pdf

Zhou, L., and Liu, W. (2005) "Broadband polarizing beam splitter with an embedded metal-wire nanograting," Opt. Lett. 30, 1434.

APPENDICES

Appendix A Equipment Specifications

DH-2000-BAL Light Source specifications (courtesy of Ocean Optics)

Weight:	3.8 kg
Power consumption:	25 W (deuterium); 20 W (tungsten halogen)
Wavelength range:	215-400 nm (deuterium bulb) 360-2000 nm (tungsten halogen bulb)
Humidity:	5-95% without condensation at 40 °C
Tungsten bulb voltage:	Adjustable from 4.5 to 11.5 volts
Lamp current:	Operating 85 V/0.3A
Lamp lifetime:	1,000 hours
Lamp voltage:	Ignition 350 V/20°
Current voltage drift:	<0.01% per hour
Current voltage stability:	<5 x 10-6 peak-to-peak (0.1-10.0 Hz)
Operating temperature:	5 °C - 35 °C
Power requirements:	85-264 V 50/60 Hz
Total power:	100 W
Warm-up time:	40 minutes (deuterium); 20 minutes (tungsten halogen)
Power consumption:	190 W maximum

http://www.oceanoptics.com/products/dh2000bal.asp

FOIS-1 Integrating Sphere (courtesy of Ocean Optics)

Spectral range: 200-1100 nm
Dimensions: 56.8 mm x 62.4 mm x 38.1 mm
Weight: 240 g
Sample port aperture: 9.5 mm
Sphere coating: Spectralon
Top cap mounts: (2) 6-32 threaded holes, (2) 8-32 threaded holes
Side mounts: SMA 905 connector for coupling optical fiber to the spectrometer
8-32 threaded hole for post mounts
http://www.oceanoptics.com/products/fois.asp

QE65000 Spectrophotometer (courtesy of Ocean Optics)

Detector Hamamatsu S7031-1006 Detector range: 200-1100 nm	Dynamic range: 7.5 x 10^9 (system), 25000:1 for a single acquisition
Pixels: 1024 x 58 (1044 x 64 total pixels); 24.6 µm square size	Integration time: 8 ms to 15 minutes
Pixel size: 24.576 µm square size Pixel well depth: 300,000 electrons/well; ~ 1.5 million electrons/column	Stray light: <0.08% at 600 nm; 0.4% at 435 nm Corrected linearity: >99.8%
	Power consumption: 500 mA @ 5 VDC (no TE cooling); 3 A @ 5 VDC (with TE cooling)
Sensitivity: 22 electrons/count for all wavelengths; 250 nm: 26 photons/count	Data transfer speed: Full scans to memory every 7 ms with USB 2.0 port, 18 ms with USB1.1 port, 300 ms with serial port
Quantum efficiency: 90% peak	Inputs/Outputs: 10 onboard digital user-programmable GPIOs
Optical Design: f/4, Symmetrical crossed Czerny-Turner Focal length: 101.6 mm input and output Entrance aperture: 5, 10, 25, 50, 100 or 200 µm wide slits or fiber (no slit) Grating options: 14 different grating options, UV through Shortwave NIR HC-1 grating option: provides 200-950 nm range OFLV filter options: OFLV-QE Other bench filter options: Longpass OF-1 filters SMA 905 to 0.22 numerical aperture single-strand optical fiber Optical resolution: ~0.14-7.7 nm FWHM Signal-to-noise ratio: 1000:1 (at full signal) A/D resolution: 16 bit Dark noise: 3 RMS counts	Strobe functions: Yes
	Connector: 30-pin connector
	Power-up time: <5 seconds
	Dark current: 4000 e-/pixel/sec @ 25 ºC; 200 e-/pixel/sec @ 0 ºC
	Windows 98/Me/2000/XP, Mac OS X and Linux with USB port; Any 32-bit Windows OS with serial port USB 2.0 @ 480 Mbps; RS-232 (2-wire) @ 115.2 K baud
	Peripheral interfaces: SPI (3-wire); I2C inter-integrated circuit

http://www.oceanoptics.com/Products/qe65000.asp

Fiber Optic Cable (courtesy of Ocean Optics)

Solarization-resistant UV/SR-VIS 190-800 nm (most efficient)
http://www.oceanoptics.com/products/premgradesol.asp

Fiber Optic Collimating Lens (courtesy of Ocean Optics)

74-UV-HT
High-temp version of 74-UV200-2000 nm
150 °CSMA 905,
6.35-mm ferrule, 3/8-24 external thread
http://www.oceanoptics.com/products/74series.asp

Omega CNi16D43-E1 Temperature Controller (courtesy of Omega)

http://www.omega.com/Temperature/pdf/CNI_Series.pdf

Appendix B Graphs and Data

The data below each graph relates to the graph shown directly above the data.

Magnesium Fluoride Results

MgF_2 550 C

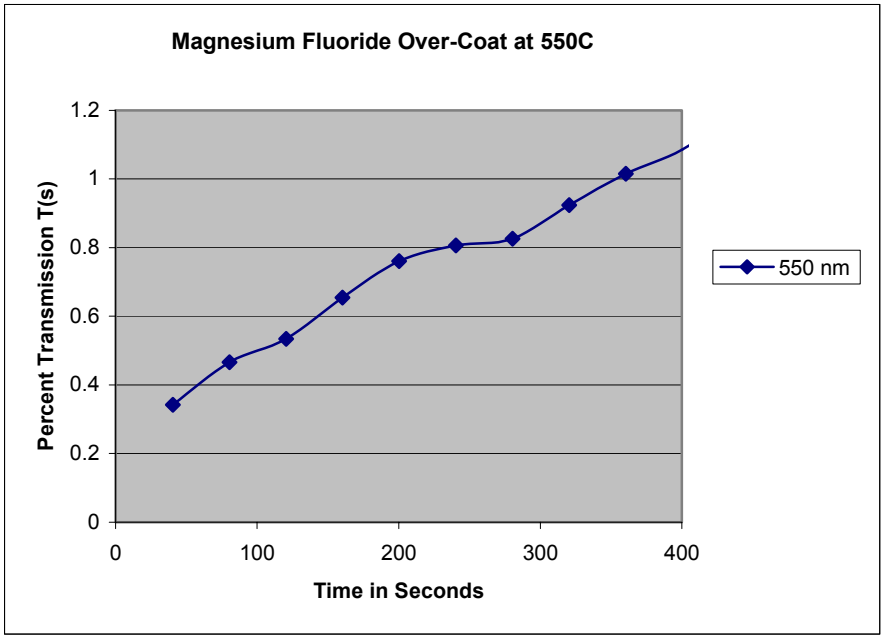

Time (sec)	Channel A
40.442	0.342202
80.438	0.466331
120.433	0.534419

160.429 0.654894

200.425 0.760613

240.422 0.806366

280.417 0.825859

MgF_2 500 C

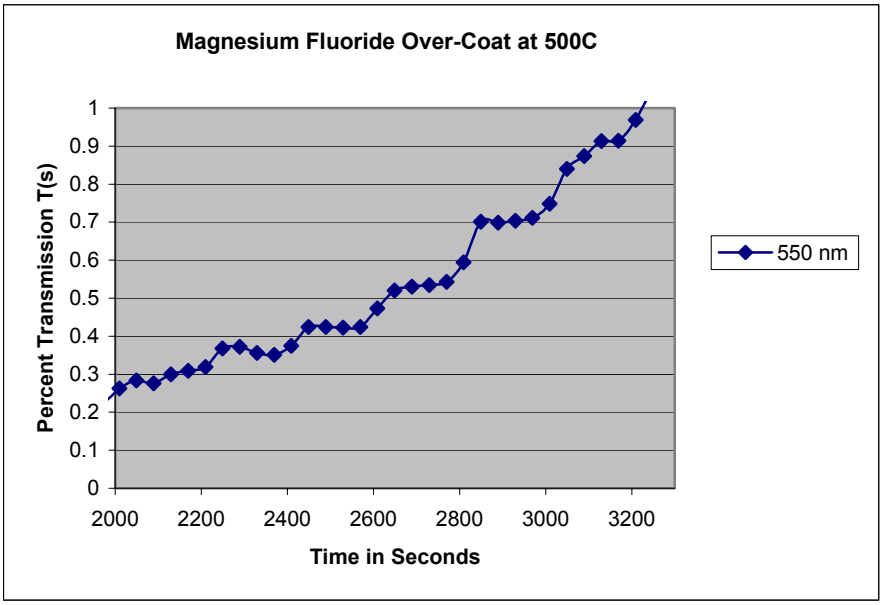

Time (sec) Channel A

2409.409 0.374398

2449.405 0.424238

2489.401 0.424371

2529.396 0.422634

2569.392 0.424104

2609.388 0.473276

2649.384 0.520042

2689.379 0.52993

2729.375	0.534473
2769.372	0.542624
2809.367	0.593933
2849.363	0.700827
2889.359	0.698823
2929.354	0.703633
2969.35	0.711517
3009.346	0.748262
3049.342	0.840459
3089.337	0.873329

MgF_2 450 C

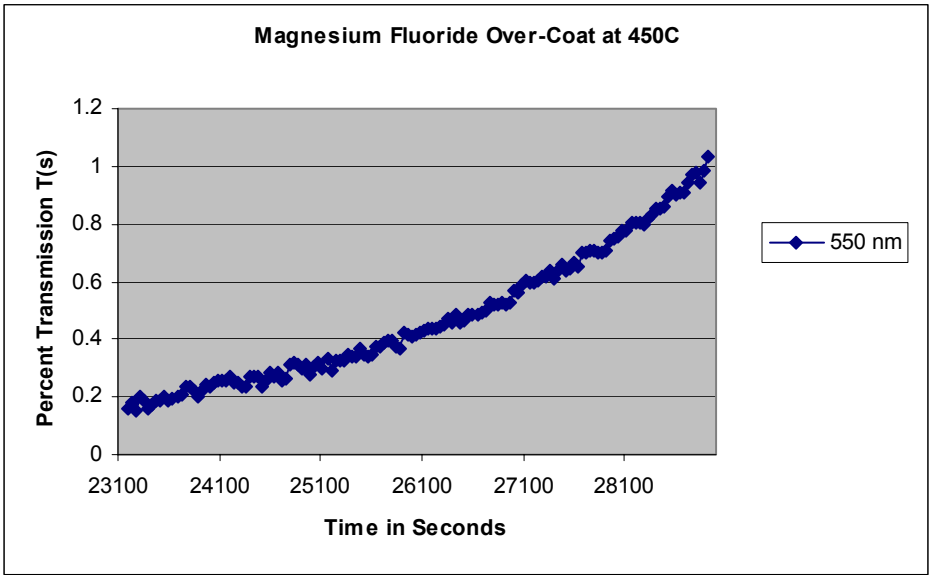

Time (sec)	Channel A
25842.1	0.372452
25882.1	0.370324

25922.09	0.419939
25962.09	0.417545
26002.08	0.4085
26042.08	0.419407
26082.07	0.426457
26122.07	0.430182
26162.07	0.440158
26202.06	0.435237
26242.06	0.436567
26282.05	0.441089
26322.05	0.44774
26362.05	0.473014
26402.04	0.457717
26442.04	0.485917
26482.03	0.455455
26522.03	0.465698
26562.03	0.483921
26602.02	0.483522
26642.02	0.487779
26682.01	0.491237
26722.01	0.498952
26762	0.527551
26802	0.522098
26842	0.519171
26881.99	0.528616
26921.99	0.519703
26961.98	0.530345

27001.98 0.571581

27041.98 0.560141

27081.97 0.586612

27121.97 0.604835

27161.96 0.596987

27201.96 0.593662

27241.95 0.601643

27281.95 0.614413

27321.95 0.615211

27361.94 0.63676

27401.94 0.611353

27441.93 0.635563

27481.93 0.656579

27521.93 0.640883

27561.92 0.645805

27601.92 0.666423

27641.91 0.653919

27681.91 0.697283

27721.9 0.698214

27761.9 0.706461

27801.9 0.70553

27841.89 0.698879

27881.89 0.70021

27921.88 0.708324

27961.88 0.739317

28001.88 0.747298

28041.87 0.758738

28081.87 0.779356

28121.86 0.777759

28161.86 0.804762

28201.86 0.805826

28241.85 0.807955

28281.85 0.799441

28321.84 0.820724

28361.84 0.83243

28401.83 0.853447

28441.83 0.85225

28481.83 0.857304

28521.82 0.892554

Silicon Dioxide Results

SiO_2 550 C

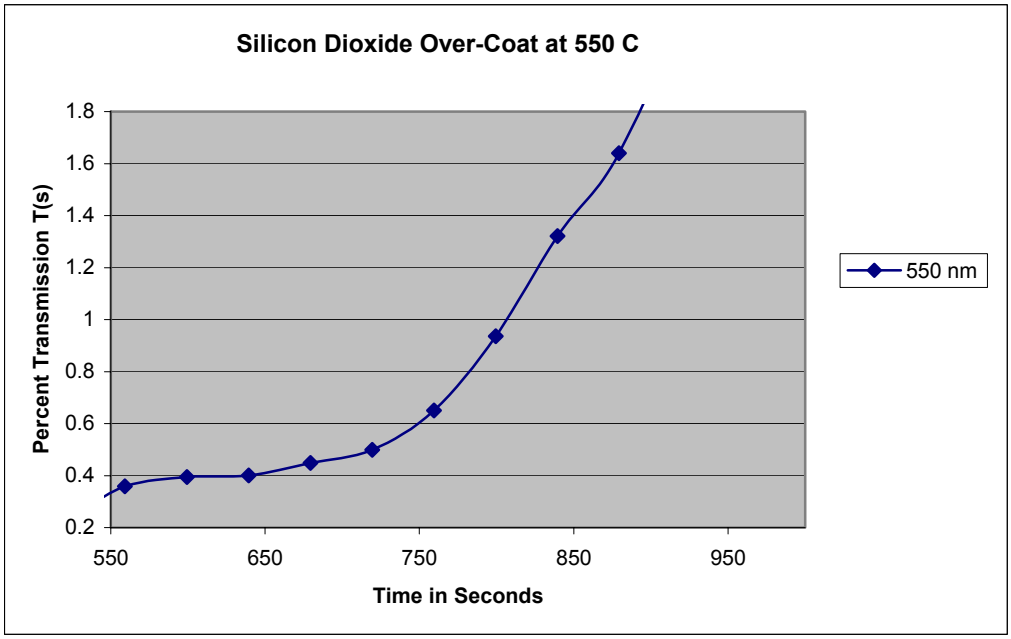

Time (sec)	Channel A
559.119	0.358249
599.315	0.394264
639.411	0.401005
679.407	0.448218
719.402	0.498603
759.398	0.649894
799.394	0.935528

SiO_2 500 C

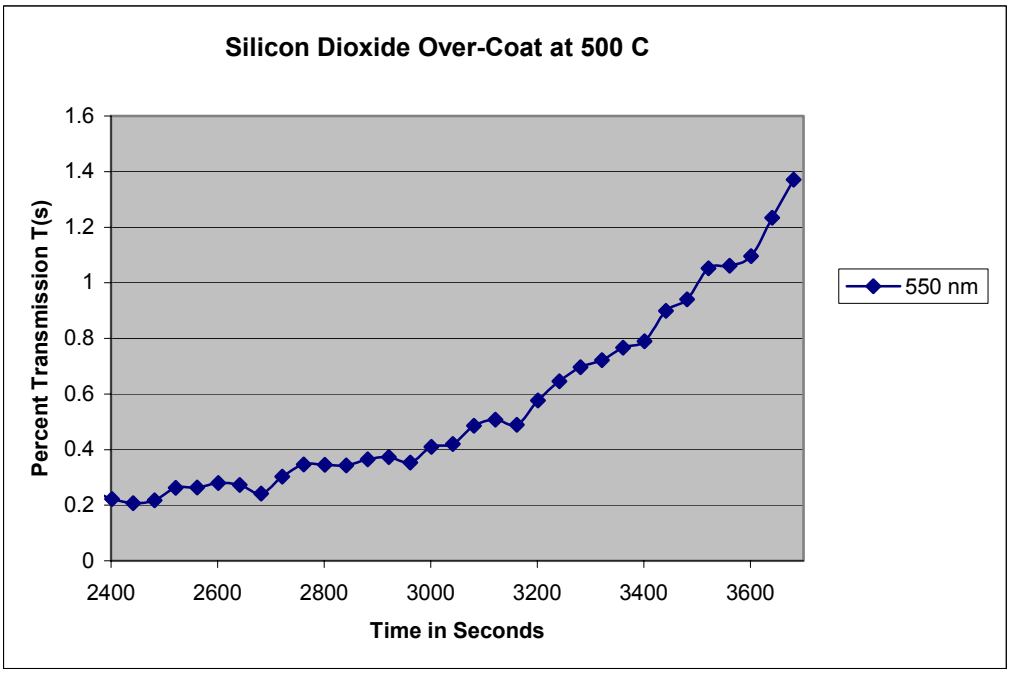

Time (sec) Channel A

2961.493 0.353178

3001.489 0.409791

3041.484 0.420243

3081.48 0.486066

3121.476 0.507836

3161.472 0.489119

3201.467 0.577159

3241.463 0.645971

3281.46 0.696906

3321.455 0.722284

3361.451 0.766745

3401.447 0.789262

3441.443 0.898477

SiO_2 450 C

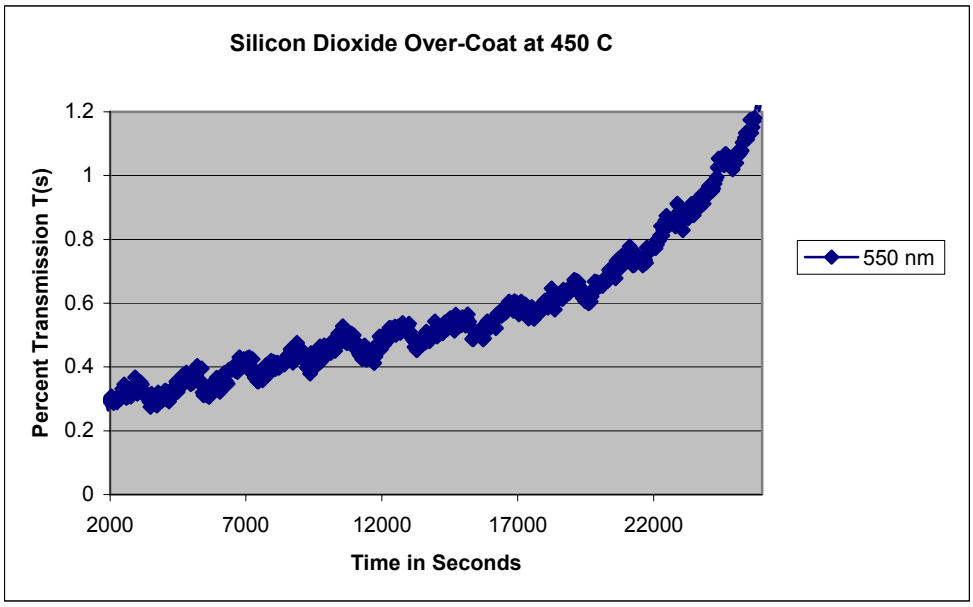

Time (sec)	Channel A
21202.27	0.731829
21242.27	0.718215
21282.26	0.71914
21322.26	0.747028
21362.25	0.73923
21402.25	0.751786
21442.25	0.734472
21482.24	0.737512
21522.24	0.738305
21562.23	0.726938
21602.23	0.718347
21642.22	0.743327
21682.22	0.736322
21722.22	0.726145

21762.21	0.775048
21802.21	0.757998
21842.2	0.761435
21882.2	0.77029
21922.2	0.777295
21962.19	0.776502
22002.19	0.775313
22042.18	0.77822
22082.18	0.772801
22122.17	0.783507
22162.17	0.800557
22202.17	0.796989
22242.16	0.811527
22282.16	0.842191
22322.15	0.811395
22362.15	0.830031
22402.15	0.845099
22442.14	0.859637
22482.14	0.874176
22522.13	0.84642
22562.13	0.843116
22602.13	0.848667
22642.12	0.850121
22682.12	0.85554
22722.11	0.867039
22762.11	0.861752
22802.1	0.840341
22842.1	0.867568

No Over-Coat Results

No Over-Coat 550 C

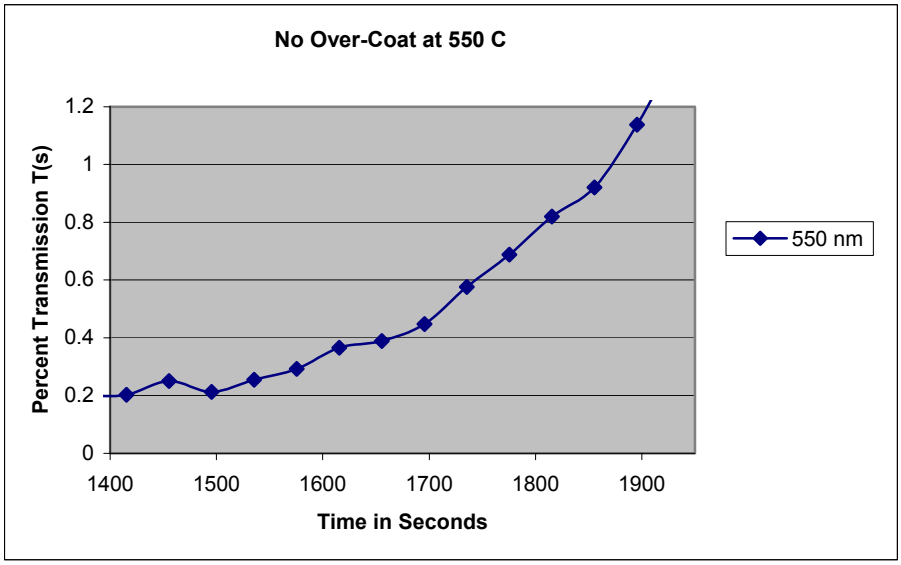

Time (sec)	Channel A
1615.481	0.365935
1655.476	0.388452
1695.472	0.447913
1735.468	0.575734
1775.463	0.687645
1815.459	0.819511
1855.455	0.921309

No Over-Coat 500 C

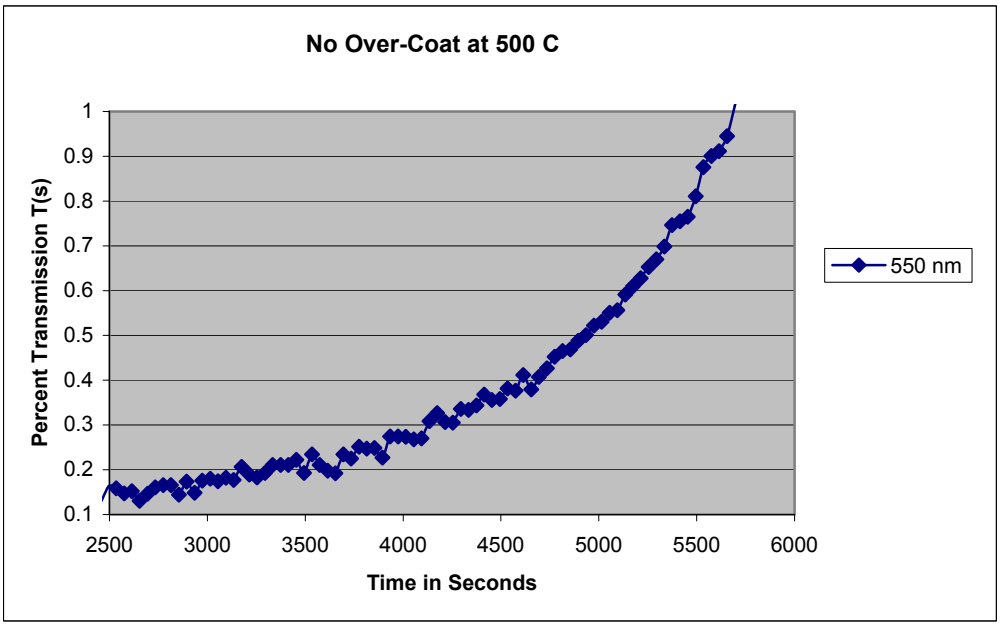

Time (sec)	Channel A
4494.269	0.358069
4534.265	0.381709
4574.261	0.3765
4614.256	0.411092
4654.252	0.379572
4694.249	0.406818
4734.245	0.426584
4774.24	0.452495
4814.236	0.465183
4854.232	0.468789
4894.227	0.487754
4934.223	0.500976
4974.219	0.522212

5014.416	0.530493
5054.411	0.550526
5094.407	0.556136
5134.403	0.591128
5174.398	0.610227
5214.394	0.62799
5254.39	0.652698
5294.386	0.670194
5334.381	0.698909
5374.377	0.746322
5414.374	0.755004
5454.369	0.765154
5494.365	0.81043
5534.361	0.875607
5574.357	0.900716

No Over-Coat 450 C

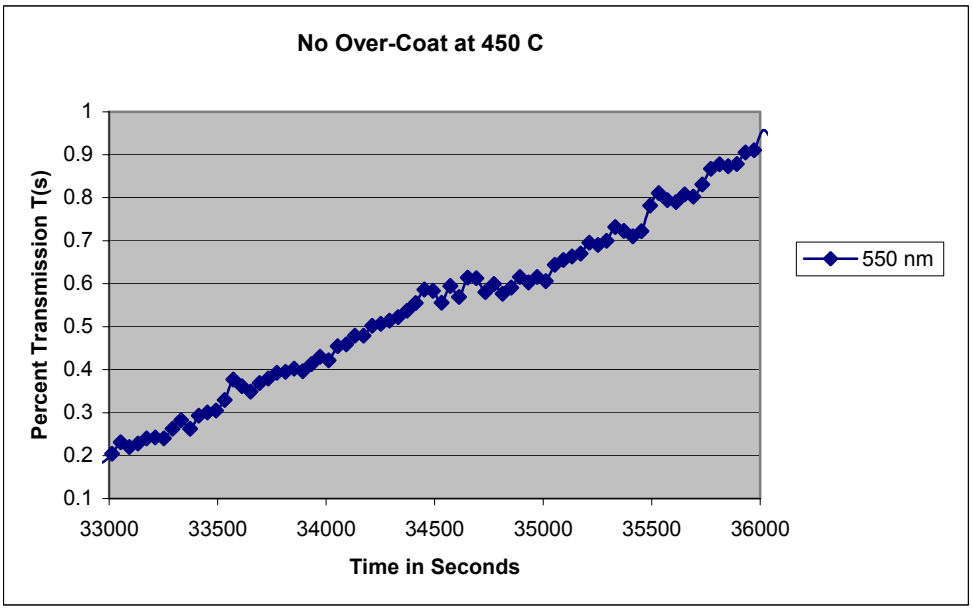

Time (sec)	Channel A
33892.51	0.39672
33932.51	0.412817
33972.5	0.430112
34012.5	0.421997
34052.49	0.454991
34092.49	0.459248
34132.48	0.479337
34172.48	0.47947
34212.48	0.502485
34252.47	0.507141
34292.47	0.514059
34332.46	0.522707
34372.46	0.537607
34412.46	0.555567

34452.45	0.586432
34492.45	0.583505
34532.44	0.555833
34572.44	0.594681
34612.43	0.569004
34652.43	0.613705
34692.43	0.612641
34732.42	0.580712
34772.42	0.59947
34812.41	0.57712
34852.41	0.590689
34892.41	0.615568
34932.4	0.60253
34972.4	0.615701
35012.39	0.606122
35052.39	0.643639
35092.39	0.655346
35132.38	0.663328
35172.38	0.669714
35212.37	0.695257
35252.37	0.690069
35292.36	0.699382
35332.36	0.731976
35372.36	0.722663
35412.35	0.710025
35452.35	0.721865
35492.34	0.781599
35532.34	0.811134

35572.34	0.794371
35612.33	0.789582
35652.33	0.807675
35692.32	0.80222
35732.32	0.830956
35772.31	0.867276
35812.31	0.87752
35852.31	0.872996
35892.3	0.87885
35932.3	0.905458